Thesis Title: Leak detection in power plant heat recovery steam generators utilising medical radionuclides.

Student Name: David Watkins

Student Number: 30742530

Degree Title: Master of Philosophy

Date Submitted: May 2018

Supervisor: Professor Malcolm Joyce

Lancaster University

1 Contents

2 List of Figures

3 Abstract

Gas-fired electrical generating plant is operating increasingly in fast response mode to meet the variability of renewable generation. Fast power turn up and turn down is required to ensure grid frequency stability. Modern gas turbines operating in combined cycle mode can achieve fast response ramp rates typically in the region of 40 MWe/min (turbine, 2018), this places increased stress on thick walled steam turbine and boiler components, leading to steam leaks and premature failure.

Established methods by which these leaks are detected rely on pressure drop testing: for power plants operating in today's fast response market conditions a pressure drop test is not possible. The first evidence of a tube leak is usually associated with a catastrophic failure of a tube necessitating an unplanned plant shutdown. To meet availability requirements, an alternative boiler leak detection system is called for.

The injection and detection of a short-lived radioactive tracer into the high pressure side of the boiler feed water circuit during operation would provide an indication of a leak in the low pressure circuit gases exiting the boiler gas stack.

This thesis examines if medical radionuclides injected into the boiler feedwater could be detected in the low pressure gas exhaust stream during the early propagation of a boiler tube leak site.

4 Introduction

Power plant boilers can develop tube leaks whilst in service. Established methods by which these leaks are detected rely on pressure testing (pressure drop test), on-line acoustic monitoring and off-line non-destructive testing (Carson & Coleman , 2009). Early diagnosis of boiler tube leaks reduce outage durations as prompt repair limits collateral damage to adjacent boiler components. Without diagnostic equipment, the first evidence of a tube leak is usually associated with a catastrophic failure of a tube necessitating an unplanned plant shutdown. Generating units that frequently cycle from start-up to shut-down are most at risk from thermally induced boiler tube leaks.

Gas-fired generating plant is increasingly operating in fast response mode to meet the variability of renewable generation. Gas turbine maintenance intervals are governed by the number of start-ups and dynamic operating hours. Operating in such a flexible response mode with frequent start-ups and shut downs has significant availability and maintenance cost implications.

Periods of plant unavailability due to boiler leaks are in the order of five to seven days to facilitate boiler cooldown, plant isolation and draining, repair and recommissioning. At current power prices of £60 per MWh, a typical shutdown can cost in excess of £3M for a 450 MW unit. The benefits of early detection aids in the planning, preparation, spares procurement, availability of suitably qualified staff and ultimately, the traded availability of the plant.

With traditional boiler leak detection methods proving unreliable for units that frequently cycle, an alternative boiler leak detection system is called for.

It is postulated that the injection of a suitable short-lived radioactive tracer into the high pressure side of the boiler feed water circuit during operation could be detected in the low pressure circuit gases exiting the boiler gas stack. Stack gases are already

monitored as a requirement of power plant environmental permits for carbon dioxide, carbon monoxide and nitrous oxide.

The difficulty lies in the selection of a suitable radiotracer that is compatible with the existing the boiler water circuit, does not contaminate boiler internal surfaces and does not present a radioactive hazard to people or the environment.

This dissertation examines the use of traditional leak detection radiotracers such as ^{24}S, ^{82}Br, ^{131}I, ^{113}In, ^{79}Kr, ^{85}Kr, ^{133}Xe, and ^{41}Ar and compares their suitability with medical radiotracers, ^{13}N, ^{18}F, ^{15}O and ^{11}C.

5 Background

5.1 Combined cycle gas turbine (CCGT) power plants

This work is focussed on the challenge associated with operating CCGT's in an electricity market that requires gas generating plant to respond quickly to fluctuating output from wind turbines and photovoltaic panels. Gas turbines operate at their highest efficiencies when they are fully heat soaked[1] and operating near maximum power output, constantly cycling power output increases the stress on components and reduces plant efficiency. Operating a CCGT power plant that is capable of fast start-up and flexible power levels requires a balance between meeting the market requirements and plant longevity.

Gas turbines can operate in two modes of operation;

- In simple cycle mode the gas turbine drives an electrical generator directly and the exhaust gas heat energy is discharged to atmosphere via a chimney

[1] A fully heat soaked turbine refers to a turbine were all internal components are operating at the same temperature. The turbine start-up procedure ensures that until all fixed to rotating components have achieved the same temperature, the control system will limit steam admission to prevent a mismatch in thermal expansion between the rotor and casing.

or exhaust stack. Gas turbines operating in open cycle mode typically can achieve cycle efficiencies of 41% (Siemens, 2018).

- In combined cycle mode, the gas turbine exhaust is used to generate steam in a heat recovery steam generator. The steam is used to drive a steam turbine providing additional energy for generating electrical power. Gas turbines operating in combined cycle mode can achieve cycle efficiencies in excess of 61% (Siemens, 2018).

5.2 Gas Turbine

The gas turbine compresses air (typically 1:15 ratio) and mixes it with fuel that is pre heated to around 250°C to increase cycle efficiency. The hot air-fuel mixture is ignited and expands through the gas turbine blades causing the gas turbine to rotate. The rotational energy drives a generator that converts rotational energy to electrical energy. Figure 1 Siemens 8000H 50Hz gas turbine, net output in simple cycle mode 450MW, net output in combined cycle mode 665MW.

5.2.1 Steam turbine delivers additional electricity.

The steam turbine uses the steam produced by the HRSG and sends its energy to the generator drive shaft where it is converted into additional electricity. Steam turbines can be connected on a common shaft to the same generator as the gas turbine is driving or in a multi shaft arrangement utilizing a separate generator. In the multi shaft arrangement multiple gas turbines can be connected to one large steam turbine which minimizes the need for multiple smaller steam turbines.

Figure 1 Siemens 8000H 50Hz gas turbine, net output in simple cycle mode 450MW, net output in combined cycle mode 665MW. (Siemens, 2018)

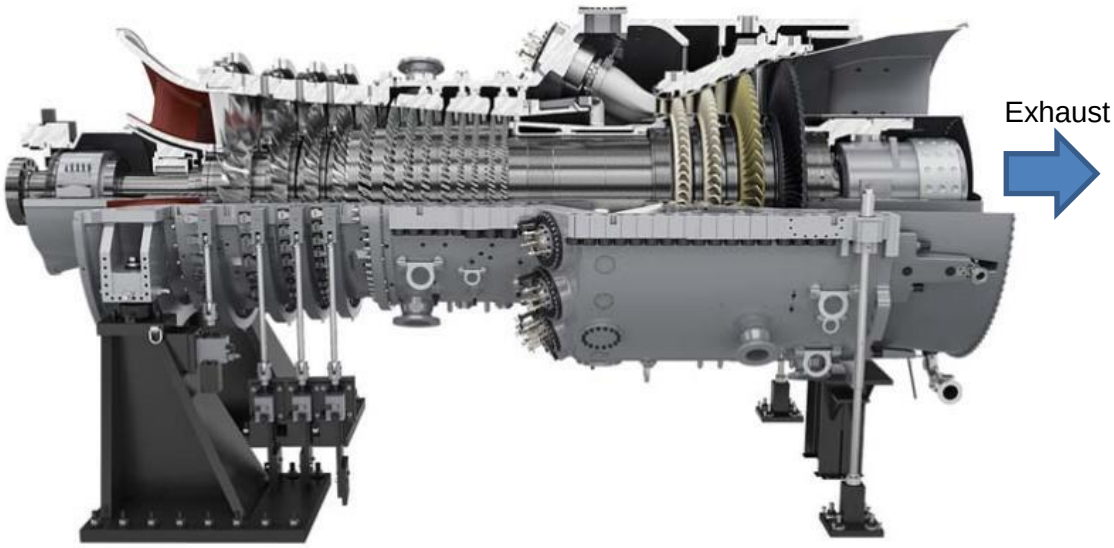

Figure 2 Siemens steam turbine, type SST – 3000 with an output of 250MW (Siemens, 2018)

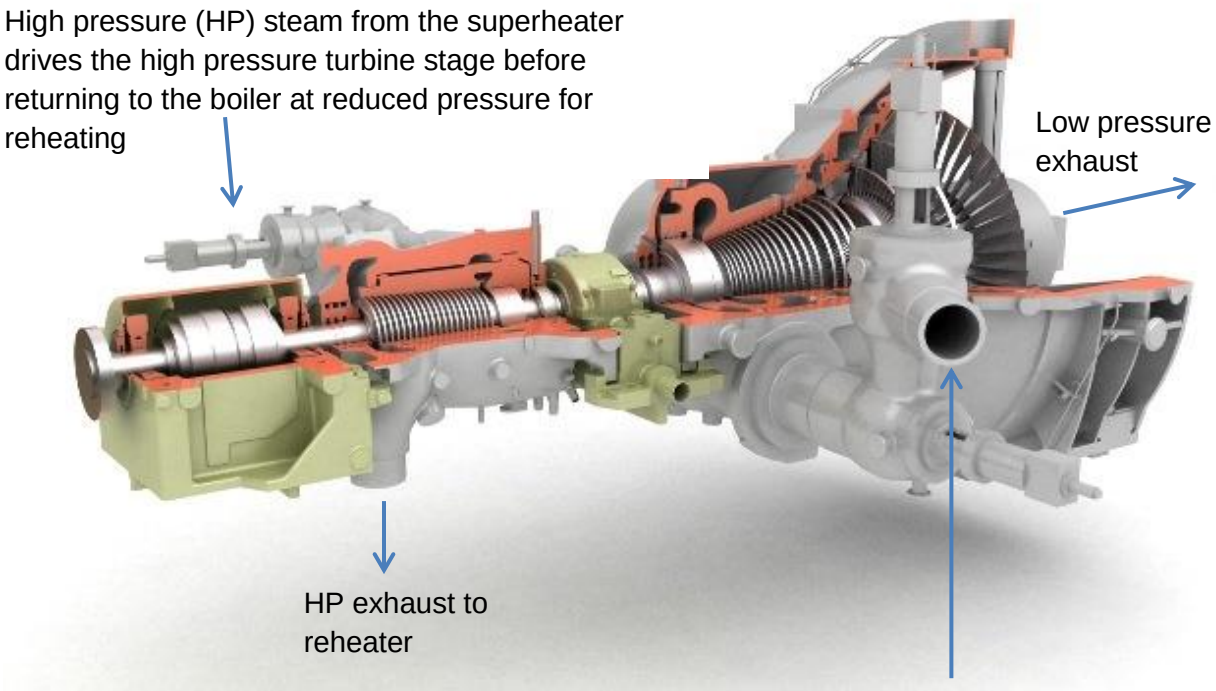

6 UK Electricity Supply Industry forecast growth 2016 to 2035

The power sector demand is predicted using the Dynamic Dispatch Model (DDM) (Department for Business, 2016). The DDM models the impact of all relevant policies, Feed in Tariffs, Renewables Obligations, Contracts for Difference, Carbon Price Support, the Capacity Auction and the Industrial Emissions Directive (IED).

The model predicts a continued decline in fossil fuel generation offset by renewable, nuclear and imported generation from subsea links.

Figure 3 Projected UK Generation and net imports (TWh) (BEIS, 2016)

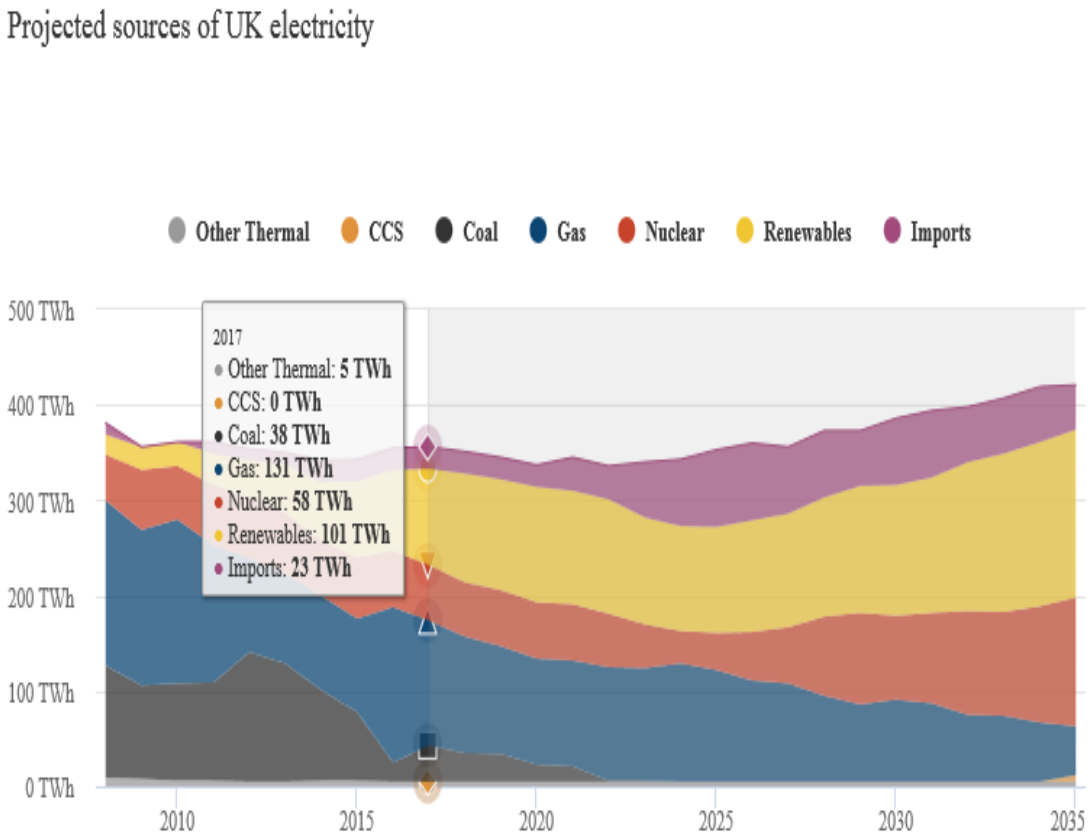

The figure shows the phasing out of coal fired generation necessary for the UK to comply with European emissions regulations. Gas fired generation is also being displaced by renewables and nuclear new build in the longer term. The current model predicts a small temporary reduction in the renewable generation in early 2020's due

to the temporary increase in gas generation to maintain system stability until additional nuclear capacity comes on line.

Traditionally, technology costs for the provision of generating future electrical power are compared on the “levelised cost of electricity” (LCOE). This method of comparing costs does not capture the current power system nuances of where and how we generate electrical power to accommodate the increasing mix of renewable energy sources.

Technologies with similar LCOE may have different effects on the power system. A power plant designed to provide energy at base load only (i.e., nuclear plants) may be of less value to the system as a power plant which can provide fast response in a system with a dependence on renewable generation.

Variable output generators such as wind; solar and tidal require a system which can accommodate their variable power output. This necessitates other generators are available on standby to be started up, shut down or ramped up/down in power to meet demand.

Power plants operate at their maximum efficiency at steady loads near their maximum continuous rating. Operating at part loads or responding to fast start-up requests reduces plant efficiency, increases costs and potentially increases plant damage. Fast ramp-up (Fast on the Fly) for a modern gas turbine power plant operated in combined cycle mode is typically around thirty minutes (Siemens, 2011) from synchronization to operation at full output.

Due to the high price of natural gas in the United Kingdom, many CCGT’s operate on a marginal basis. Having been costed, designed and built to fulfil base load operation many have been reduced to fulfilling peak load lopping. It can be uneconomic to run the plant outside of periods of high system demand when prices are high.

Gas turbines operated in simple cycle mode (i.e., without a heat recovery steam generator and steam turbine) are able to increase power rapidly, load increases in the order of forty megawatts per minute can be achieved. Operating a gas turbine in simple cycle mode increases the cost of generation due to the low cycle efficiency (~41%). (Siemens, 2018). Simple cycle machines are therefore only cost effective as “peak loppers”, i.e., as machines that run to meet system demand highs.

Gas turbines operated in combined cycle modes at steady load factors can achieve over 61% cycle efficiency. (Siemens, 2018). The penalty for operating in combined cycle mode and incorporating fast start up ramps is that the thick-walled, steel components, such as boiler headers, steam drums and steam turbine components suffer increased thermodynamic-induced stress and increased low and high cycle fatigue.

In summary, the current energy mix of increasing renewable generation has to have flexible, fast response generating plant on standby. Gas turbines are currently the favoured method to provide this flexibility. Operating gas turbines in fast start-up mode increases plant availability however this also reduces plant life due to increased component stress.

Figure 4 Fast start mode – improved start up sequence increases power output (Siemens, 2011)

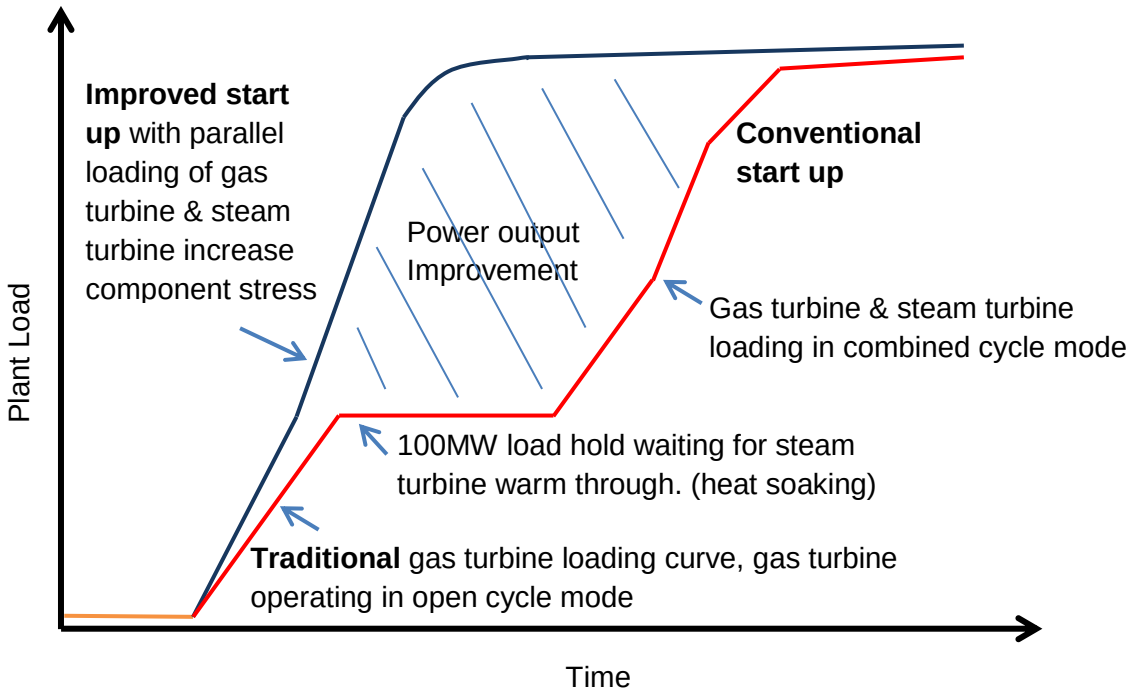

Traditional, low-stress start curves for gas turbines ramps the gas turbine up in simple cycle mode (open cycle) to 100 MW after sychronization with the grid. The gas turbine then warms through the boiler components until it has steam conditions suitable for admitting to the steam turbine without cooling the steam turbine cylinder chests. This requires steam temperatures greater than the steam turbine internal components because steam admittance with lower temperatures has the potential to shrink the rotating components which have a lower mass than the static casing. Shrinkage of the rotor can lead to differential expansion issues between fixed and rotating parts with catastrophic results.

Once steam temperatures are sufficient to avoid shrinkage, the operator admits steam to the steam turbine and the unit is now operating in combined-cycle mode, with the steam turbine augmenting the gas turbine mechanical input to the generator. As the gas turbine load is further increased, the greater exhaust gas flow through the boiler elevates steam temperaures, causing increased output from the steam turbine.

In fast start-up mode, the gas turbine has an increased power ramp rate and the steam turbine is loaded in parallel with the gas turbine instead of delaying until the steam temperature is sufficient to prevent rotor shrinkage. The benefits of this approach are a reduced time to achieve maximum load, increased generation revenue but increased stress induced fatigue on boiler and steam turbine components.

Figure 5 Change from Drum type boilers to once-through design "Benson" boilers reduces the number of thick walled components subject to stress. (Siemens, 2011)

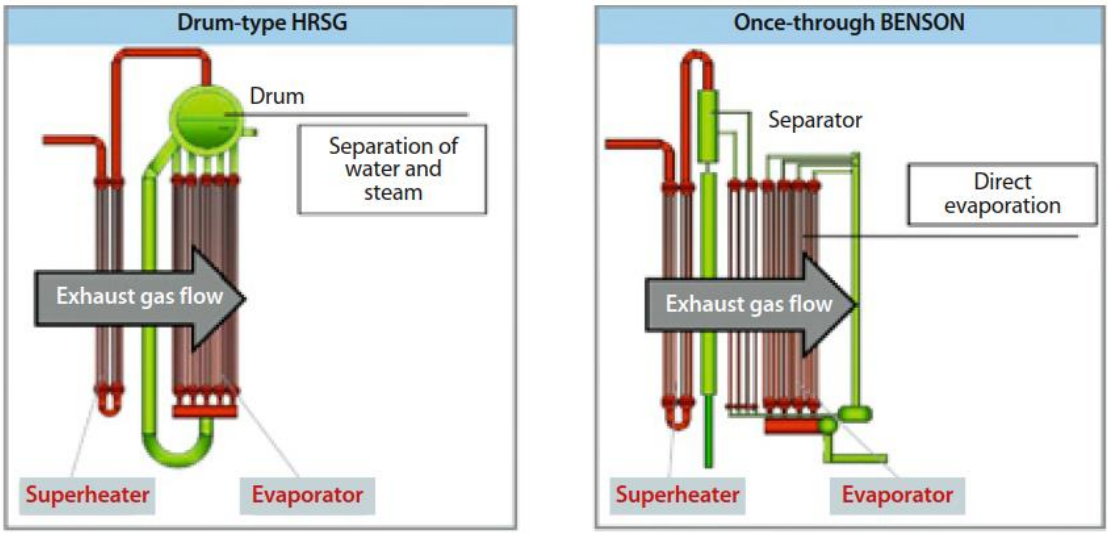

Designing the boiler to operate without a steam drum has the advantage of reducing the start up and ramp up time of the unit because the thick walled boiler drum is removed. Steam evaporation is carried out directly in the evaporator tubes thus enabling a faster ramp up as stress induced failure of the boiler drum is removed from the stress calculation model which currently limits the ramp up rate.

6.1 Start instruction from National Grid

Each generating unit submits a notice to deviate from zero (NDZ) to the National Grid dispatch and balancing mechanism, where the NDZ is the time from receiving an instruction to generate from National Grid to synchronizing the machine and starting to generate power (Grid, 2010). The shorter the NDZ quoted by the power plant, the

higher up it is placed in the merit table. Machines at the top of the merit table have a greater likelihood to be called first by National Grid to meet system demand because they can respond faster.

Any unavailability of the power plant caused by boiler leaks has a catastrophic effect on profitability. With average wholesale power prices of £60 per MWh, a 450 MW unit can potentially lose more than £3,000,000 for a five-day shutdown to repair a tube leak.

Any early detection of tube failure can help reduce downtime and increase profitability for marginal gas turbine plant.

7 Heat Recovery Steam Generators

The fundamental purpose of a heat recovery steam generator (HRSG) is to extract the useful energy in waste heat from the exhaust of a gas turbine. Modern gas turbines, such as the Siemens SGT5 – 4000F, have an exhaust temperature of 590°C. The HRSG is designed to extract as much of the heat as possible from the exhaust gas before it is ejected to atmosphere.

The HRSG consists of multiple passes of heating elements (tube banks), which produce process steam for consumption in a steam turbine. Each stage has a specific design criterion: economizer, evaporator, superheater and reheater. The stages are arranged to recover heat from the gas turbine in the following order (hottest section first): superheater, reheater, evaporator and economizer.

Figure 6 Heat Recovery Steam Generator (HRSG) utilizes exhaust gases from gas turbine to produce steam (GE, 2018)

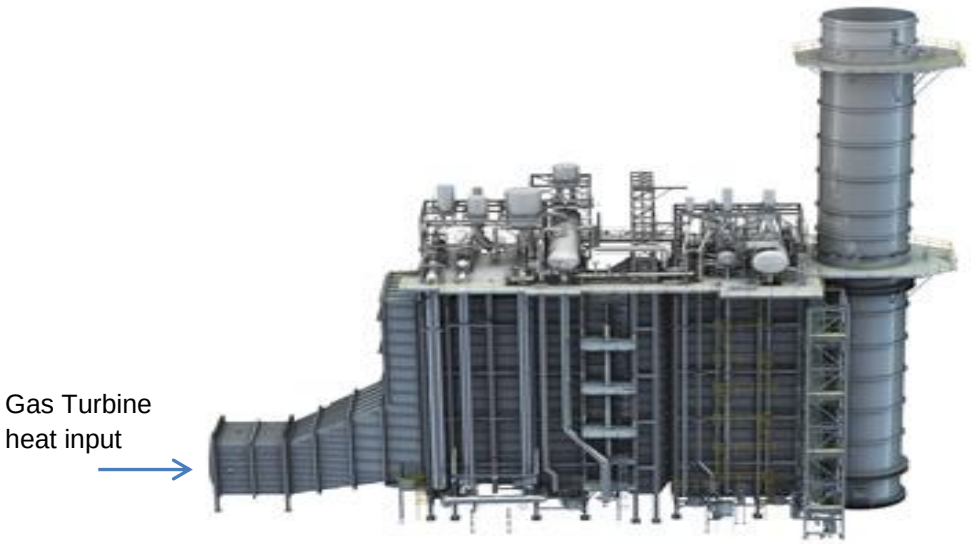

Boiler inlet gas temperatures of 590°C are reduced to 75°C at the economizer (boiler outlet) section of the boiler by each section of the boiler transferring heat to the tube banks. Final boiler exit temperatures are closely controlled to ensure that the gas dew point is not reached since if this were to occur, it can allow sulfuric acid to form on boiler components which affects boiler integrity. The natural gas fuel is the source of the sulphur and its composition is monitored for sulphur content and the exhaust temperatures adjusted accordingly.

The figure below shows the typical air/gas mass flow through a modern gas turbine. The compressor increases the air pressure and temperature through compression and adiabatic heating until the air is mixed with heated natural gas in a combustion chamber and ignited. The hot exhaust gases pass through the power turbine section causing rotation before being exhausted to the heat recovery steam generator.

Figure 7 gas turbine basic mass flow. (Siemens SGT5-4000F V94.3 A2)

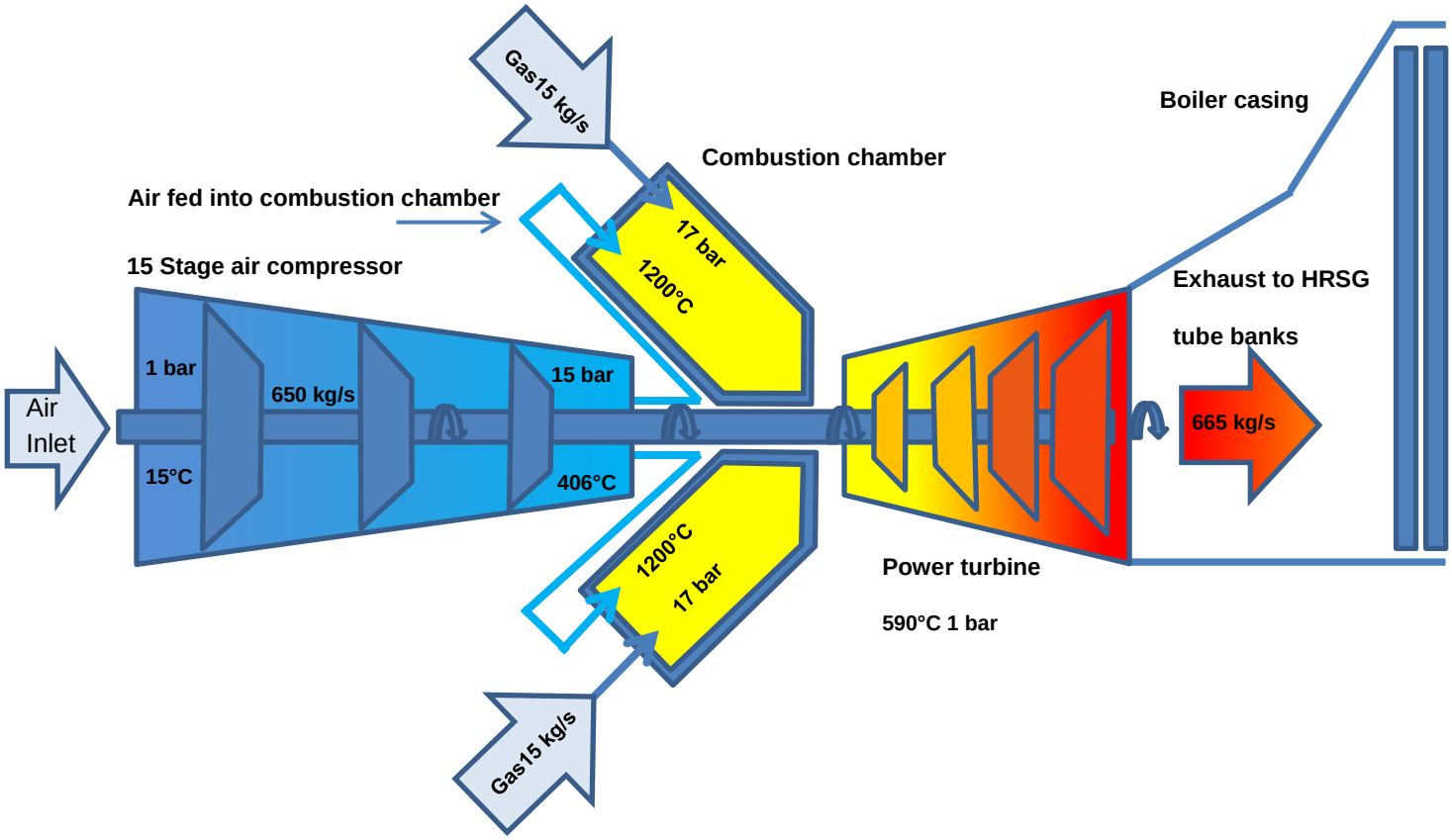

7.1.1 HRSG Complexity

Heat recovery steam generators and their auxiliary steam systems are becoming increasingly complex. Typically, a HRSG has three pressure stages, a high-pressure (HP), an intermediate-pressure (IP) with a reheater and a low-pressure (LP) boiler. Each stage has its own specific manufacturing materials (steel composition) of construction to suit the corresponding operating temperatures and pressures and water chemistry requirements.

HRSG users' groups regularly report that tube leaks are emerging as a major issue facing plant availability (Kilburn, 2007). Tube leaks can also trigger subsequent damage to other components in the HRSG, which can be even more troublesome and more costly to repair than the initial leak.

Ron Meyer, Principal Engineer and Aftermarket Product Manager for Deltak LLC, explained that '*nearly half of all HRSG tube leaks occur in the economizer section, and that they typically are caused by fatigue, corrosion fatigue, or freeze damage. Another 25% or so occur in the superheater or reheater sections, often near the tube-to-header welds'* (Kilburn, 2007).

For power plant operators, the major challenge is to find tube damage while it is still in a precursor state before it escalates into a major leak. Previously operators have used straight-wave ultrasonic testing (UT) to measure tube-wall thickness on a regular basis and thereby monitor corrosion damage before it grows into a full-fledged tube leak (Kilburn, 2007).

HRSG's operate with finned tubing which limits the effectiveness of UT for tube-thickness measurement. The finned tubes prevent the close coupling between the UT probes and the tube surface. Secondly, UT requires internal access to the boiler structures rendering the plant unavailable whilst the inspections are conducted.

Because of the limitations of UT, most tube damage in HRSGs is not detected until it presents itself in an actual leak with the catastrophic boiler damage consequences. Detecting and pinpointing the location of the leak prior to this stage is difficult.

UT is not an effective method for detecting leaks at the header to tube welds, because many welds are not assessable once built and inspection schedules to test welds would result in uneconomic outage durations.

Figure 8 HRSG finned tube showing the fins attached to the external tube surface which increases the surface area of the tube, aiding in heat transfer.

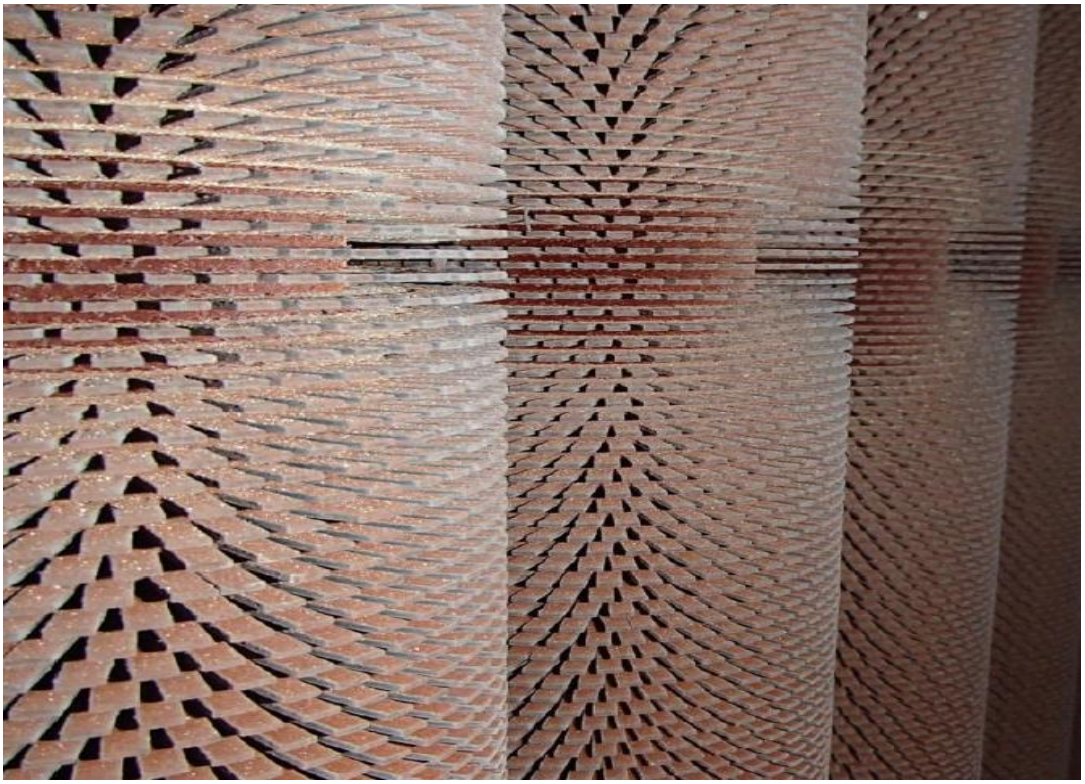

Figure 9 Tube wall showing banks of finned tubes, this is the first tube wall to interact with the exhaust flow from the gas turbine and has the highest heat loading (Superheater section).

When the HRSG is operating at load, water may be detected draining from the casing for significant leaks, checking mismatch between steam flow and feedwater

flow, changes in the stack plume, and sudden difficulty in maintaining water-chemistry parameters are other methods.

7.2 Boiler failure mechanisms

Tube failures are classified as in-service failures in boilers, these failures can be grouped under six major causes:

1. Lack of quality control
2. Water side corrosion
3. Erosion
4. Fire side corrosion (high temperature corrosion)
5. Stress rupture
6. Fatigue

For heat recovery steam generators, the main failure mechanisms are lack of quality control and water side corrosion. Erosion, fire side corrosion, stress rupture and fatigue are more prevalent in traditional coal-fired boiler plant. Coal-fired boilers are subject to erosion from pulverised fuel (coal), fire side corrosion from ash build up and fatigue from plant that cycles everyday over decades of use.

7.3 Lack of quality control

Over the first few years of operation, quality control issues are the predominant failure mechanism in HRSGs. The majority of failures occur at tube header sites where vertical tubes are welded to water or steam headers that make up each section or bank of tubes.

Figure 10 Boiler tube weld failure site, tube to header weld.

The figure above shows a section of the underside of a boiler header where vertical tubes are welded to the header. Access to the underside of the headers is restricted by boiler structural steelwork and adjacent header tubes.

Thermal cycling of the boiler causes long headers to bend due to differential expansion as the plant starts-up and shuts down. Boiler headers are designed to reduce the magnitude of bending by using multiple short headers. The weld repair shown in the figure was difficult to access as the failed area of weld was located on the underside of the header.

Figure 11 Boiler header showing vertical tube array underneath.

Figure 12 Boiler tube failure site, header access area is between support structure and tube header.

Figure 13 Repaired welded area located underneath the header.

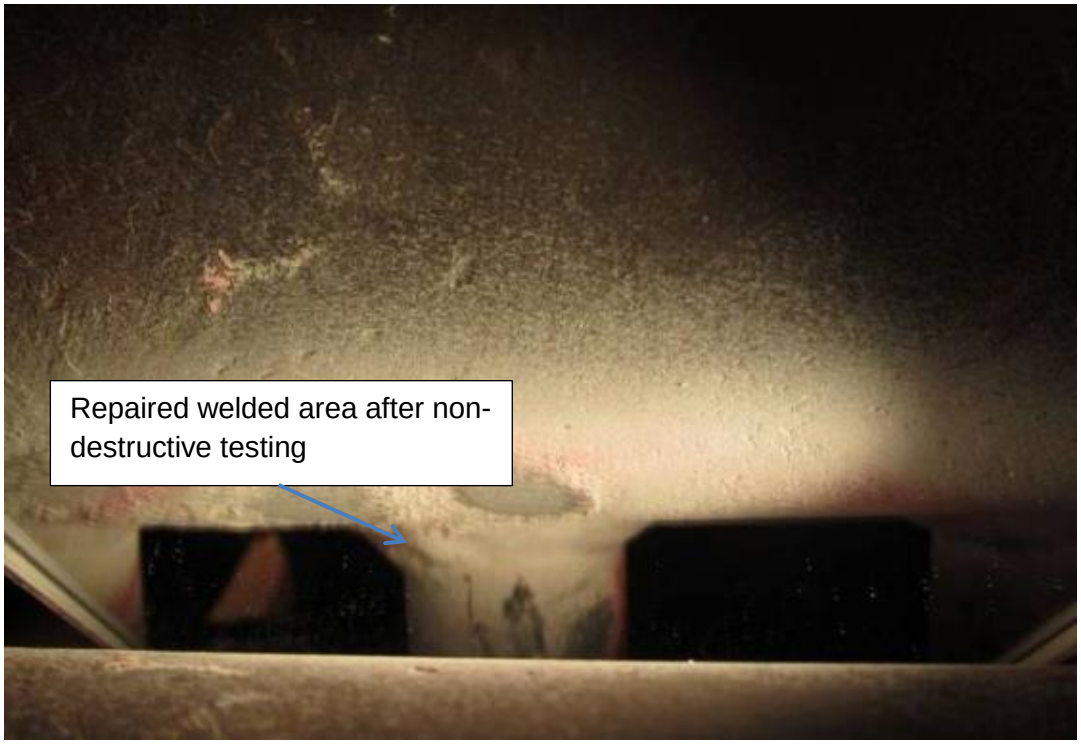

7.4 Waterside corrosion

Water side corrosion can occur after a relatively short operating period. Significant reductions of the wall thickness of boiler tubes have been observed in power plants with operating periods of eight years, (S.W Liu, 2017). The selection of material for the construction of boiler tubes depends on temperature environment that the tube will operate in. Higher quality steels are used in areas subject to higher temperatures. Superheater and reheater sections use a higher chrome molybdenum percentage than evaporator and economiser sections. The lower chrome molybdenum steels are subject to increased water/steam erosion conditions in the diphase region.[2]

To counter aggressive corrosion, chemical regimes follow standard alkaline operation with a pH >9.6 using ammonia injection and an oxygen-scavenging chemical such as hydrazine to remove dissolved oxygen from boiler feedwater.

[2] Diphase region – A region where either water or steam can exist depending on the temperature of the boiler.

Sodium phosphate (General Electric, 2012) is also used to dose the drum areas of the heat recovery steam generator to remove minerals, sodium, potassium, calcium, iron, silica and magnesium. Alkali metals are corrosive in highly-superheated steam conditions and calcium, magnesium, iron, silica cause scale.

Following this chemical regime caused several issues with caustic corrosion and acid phosphate corrosion in the lower temperature and pressure economizer regions. The most susceptible areas are in the region of elbows and bends where flow velocities are highest. Flow accelerated corrosion (FAC) affects the carbon steel tubing carrying deoxygenated water or wet steam. For economic reasons, low chrome (1Cr-0.5Mo) steel is used in the lower temperature areas of the boilers due to cost advantages. The use of higher chrome molybdenum steels alleviates FAC but increases construction costs.

The oxygen removal regime by using oxygen savaging chemicals has been altered to help with preventing FAC. Latest research has found that the addition of a small amount of oxygen into the boiler feedwater has been found to significantly reduce FAC. This is counter to traditional water chemistry practices which removed oxygen by the admission of hydrazine; this process is called All Volatile Treatment using Oxygen (AVT- O).

Figure 14 Start of Flow Accelerated Corrosion of the internal radius of an economizer tube.

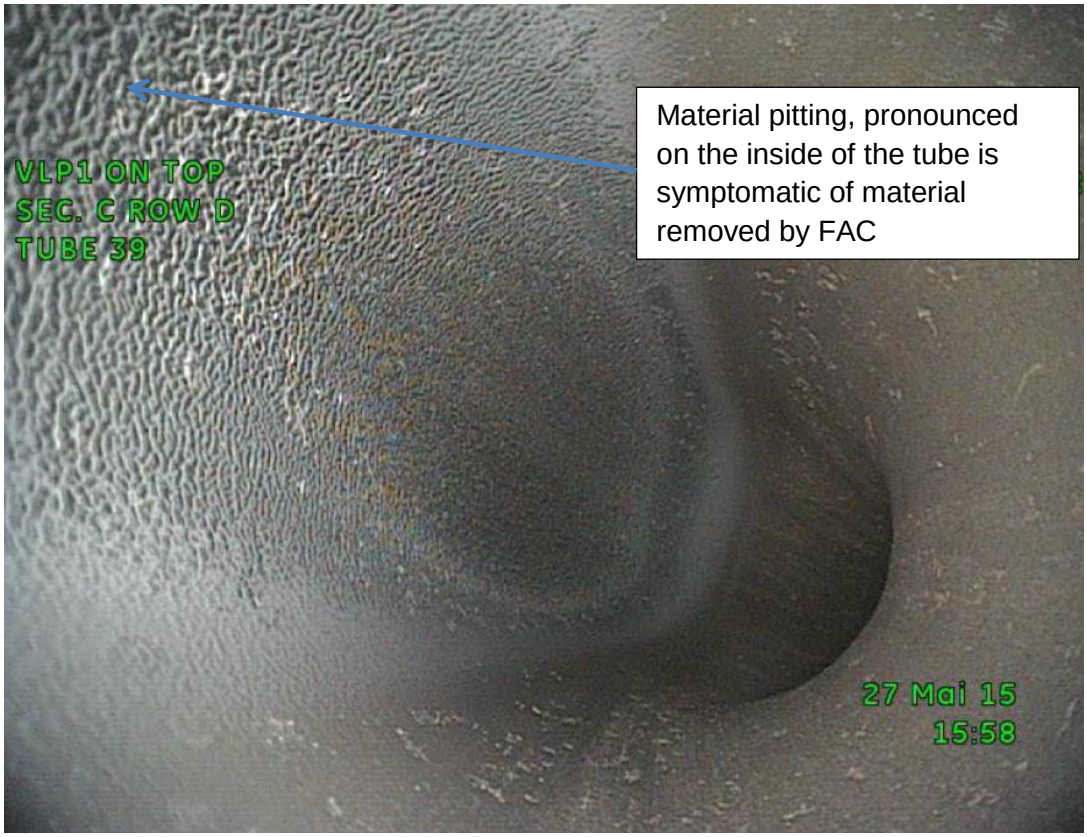

AVT - O treatment still utilizes a high-pH regime based on ammonia dosing but introduces small quantities of oxygen into the feedwater, a fundamental change from scavenging with hydrazine.

The oxygen helps with the formation of a thicker protective layer of hematite (Fe_2O_3) on top of black magnetite (Fe_3O_4), both layers help protect removal of the oxide layers of low chrome steels and thus reduce FAC.

7.5 Acoustic boiler leak sensors – Passive Acoustic Tomography

In-service monitoring utilizing on-line acoustic type steam leak detectors have also been used in coal fired boilers. Acoustic detectors are normally fitted during construction of the boiler. When a pressurized fluid escapes from a boiler tube or header it generates an acoustic emission which travels through the component structure and is transmitted via boiler gases. Small boiler leaks generate high-frequency sound emissions and as the leak size increases, the frequency of the

sound falls into the normal acoustic hearing range. By the time that a leak is in audible range of the human ear, it has usually already caused significant collateral damage to adjacent boiler components.

Figure 15 Basic system configuration of acoustic leak detection equipment.

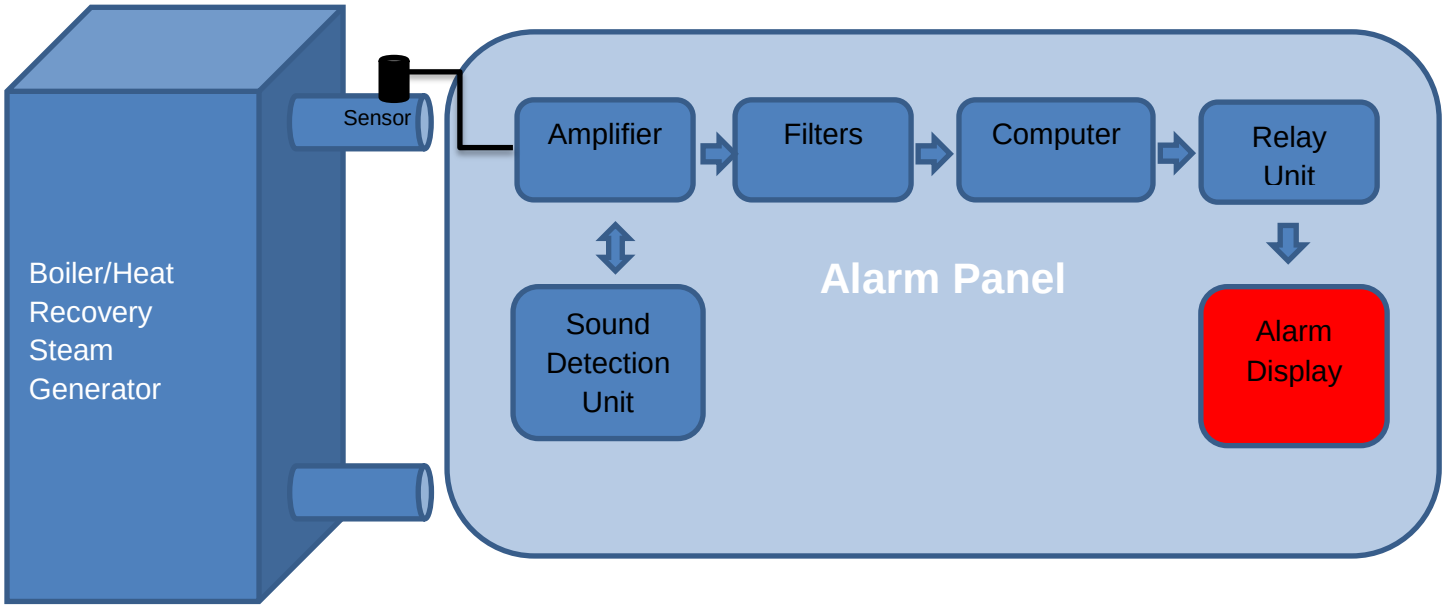

Figure 16 Multiple sensor positions are required in the boiler (Procon Engineering, 2017).

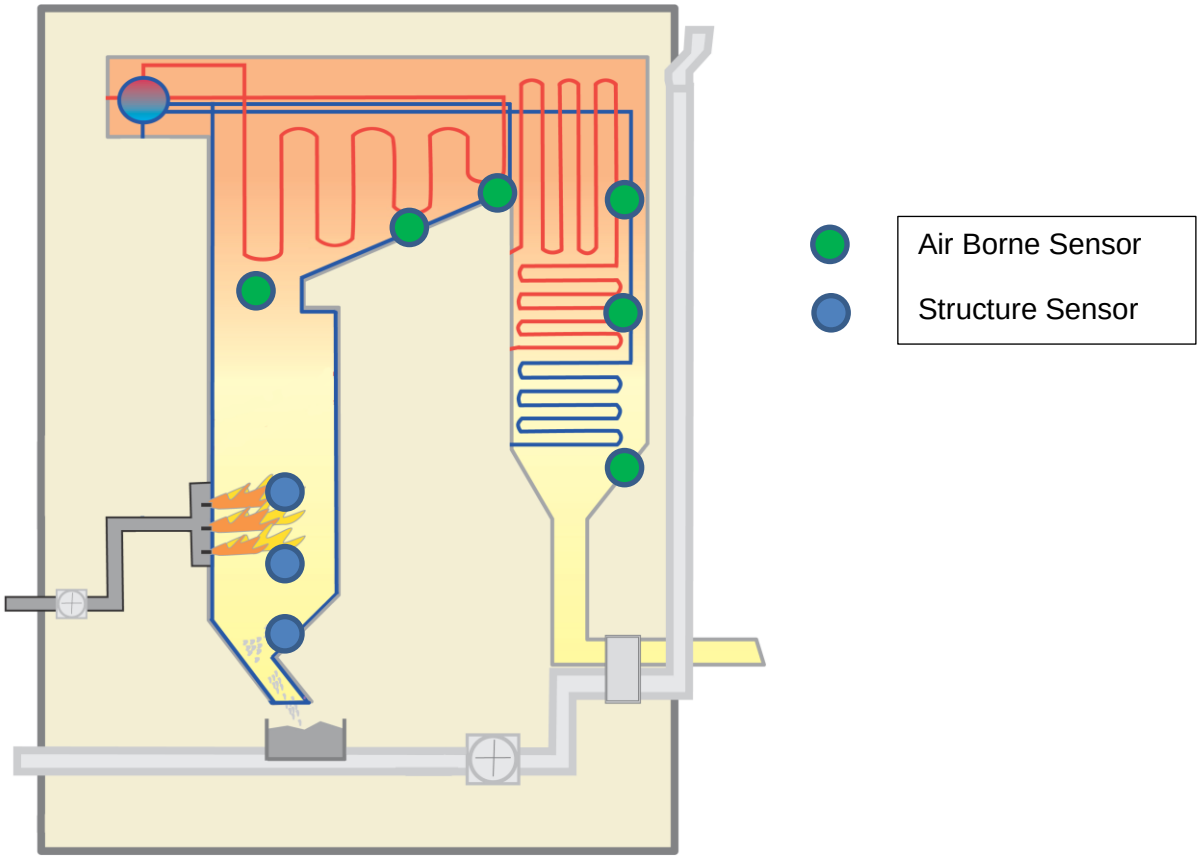

Acoustic sensors need to be tuned initially to the specific boiler on which they are used; regular re-tuning is also required to ensure that the system does not present false alarms to the operators. Operating experience on a Babcock and Wilcox boiler at the Gaston power plant provided mixed results (Studdard & Arrington, 1992) which are summarized below.

The installed system initially failed to register any response to internal boiler activity such as soot-blower[3] cleaning of the boiler tubes. This is a routine activity on steam boilers: high pressure steam is blown on to the boiler tubes via a remotely-operated lance to remove deposits. The acoustic system failed to register this significant soot-blowing activity. The waveguide assemblies required cleaning and maintenance

[3] Soot blowers are steam lances; they are inserted into the boiler spaces by a chain driven mechanism. After insertion, high pressure steam is injected from the lance tip which dislodges soot/ash from the boiler tubes, this improves tube heat transfer.

three times per week in order to function correctly, which is unacceptably high for a fixed monitoring system.

Installed equipment located close to the boiler casing suffered repeated failures due to the high radiated temperatures (>250°F, 121°C). Modifications to the system to relocate the temperature sensitive preamplifiers improved system reliability.

Most acoustic leak detection systems were fitted to the large steam boilers of coal fired power plants built by the government-owned, Central Electricity Generating Board in the UK. Since privatization (April, 1991) of the electricity supply industry in the UK, no new large coal generating power plants have been built and the acoustic leak detection technology for coal plants has stagnated.

The International Atomic Energy Agency (IAEA, 2009) quote that acoustic leak detection technique is limited to detecting leaks in the order of 10^{-3} mbar・l/s. This technique is not recommended for on-line leak detection in heat exchangers because of industrial noises and interferences providing false positives.

Acoustic systems are not normally installed by the original equipment manufacturers (OEM), as to do so could potentially infer that the boiler is prone to leakage and therefore unreliable. They are normally retro-fitted when the system in question has caused losses associated with boiler tube failures. Determining when to fit such systems is driven largely by the unreliability of the boiler and the scale of loss associated with the loss of production.

One possible solution to detecting boiler tube leaks is to utilize a system that does not necessitate a high capital outlay or which does not increase the maintenance burden and which can be used to detect small-magnitude leaks before they result in an unplanned outage.

8 Leak detection in heat exchanger systems using radioactive tracers.

In highly complex, large-capacity chemical facilities, it is necessity to minimize process down time. Because down time is expensive, this has led to an increased use of radiotracer techniques for leak detection. Radiotracer techniques can be very sensitive and effective for on-line leak detection, especially in heat exchangers and underground pipelines.

Radiotracers enable the early detection of small leakages before these develop into major process issues or environmental incidents. The International Atomic Energy Agency (IAEA, 2009) quote that radiotracer methods used for on-line leak detection in heat exchangers and underground pipelines can achieve detection limits up to 0.1% of stream flow.

Radiotracer methods are non-intrusive techniques for the early detection of leaks in heat exchangers. The benefits of using radiotracer methods are: reducing shutdown time, assurance of safe operation, protection of the environment from pollution and the avoidance of significant, unexpected costs. The same benefits are linked closely to the generation of electricity using steam heat exchangers.

Figure 17 Typical shell and tube heat exchanger arrangement (IAEA, 1995).

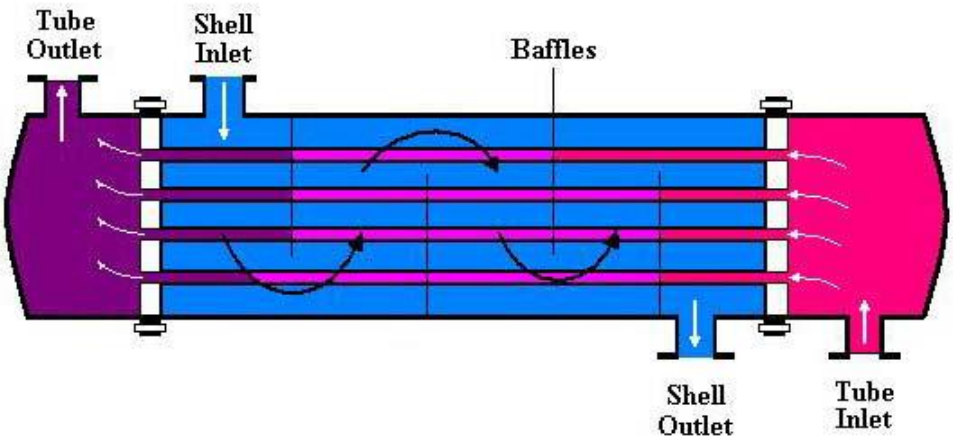

8.1 Advantages of radiotracer tracer leak detection

Radiotracer leak detection offers the possibility of producing on-line measurements that provide information in the shortest possible time. The emission of radiation is a specific property of the radioisotope injected into the system and is not affected by interference from other materials in the process; thus radiotracers have strong resistance to the severe process conditions that heat exchangers encounter.

Extremely high detection sensitivity for small concentrations of radiotracer can be achieved: for instance, the IAEA quote (IAEA, 2009) that some radiotracers may be detected in quantities as small as 10^{-17} grams. Leak detection using a radiotracer method is sensitive and can measure leak flows up to 10^{-10} mbar l/s.

8.2 Principle of operation

In a typical tracer process, a small amount of radioisotope is injected into the high-pressure side of the heat exchanger. Two radiation detectors are used to monitor its movement through the heat exchanger. The inlet detector mounted on the high-pressure side measures peak and time, whilst the output detector mounted on the low-pressure side detects the radiotracer that has infiltrated into the lower pressure side.

High pressure leakage is detected by the “subsidiary leak” or bypass leak, preceding the main peak. The main peak corresponds to the main flow of the fluid through the system (residence time). The leakage rate is the percentage of the area of the leakage peak to the sum of the areas of the leakage and main peaks.

Figure 18 Example of peaks generated at various sample points in the heat exchanger using 4 detectors (IAEA, 2009).

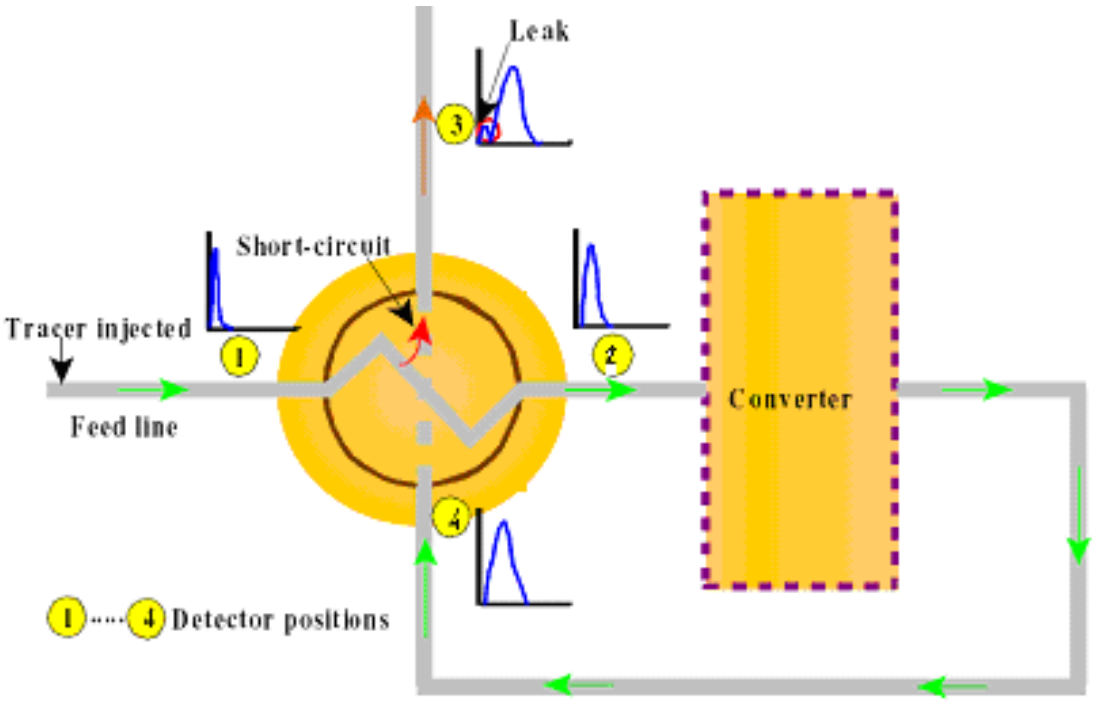

8.3 Using radioactive tracer particles in a circulating fluidized bed to determine hydrodynamics of combustion

In a 1999 paper, the Department of Chemical Engineering at the Technical University of Denmark (Weigang Lin, 1999) reported the use of a radioactive tracer to solve combustion problems in a circulating fluidized-bed (CFB) boiler.

This technology has been used widely for the combustion of coal and other solid fuels, due to its fuel flexibility and low emission levels of SO_2 and NO*x*. However, the interaction between sulphur capture and NO and N_2O emissions is complicated and the movement of the fuel particles partly determines the fate of the volatiles that are released. These phenomena show the importance of understanding the hydrodynamics of CFB combustors in order to discern the key factors to optimize the combustion system with respect to minimising harmful emissions.

Radioactive tracer particles were injected into an 80 MW CFB boiler in an attempt to determine the combustion path with a set of successive scintillation detectors located at different parts of the boiler. The results show that there are significant differences of the response signals when boiler loading changes. A model was also developed to obtain information from the experimental data. The average particle velocities in the furnace have also been estimated using the same methodology.

In the test, ^{56}Mn was chosen (having a half-life of 2.6 hours) as the isotope for the experiments; particles of magnesium containing alumina silicate were chosen as artificial tracers. A part of the magnesium in the ceramic/glass particles is substituted by manganese, which is activated by irradiation of the particles in a neutron flux.

The contribution of ^{56}Mn in the particles is sufficient to give a detectable level of radioactivity and the density of particles was close to the density of the bed material in the boiler. The particles were dispensed in a portion of sand and injected into the plant with a probe in batches. The response signals of the impulse injection were measured using two sets of 16 thallium-doped, sodium iodide (NaI(TI)) scintillation detectors.

Figure 19 Circulating Fluidized Bed showing injection points of the radioactive tracer (Weigang Lin, 1999).

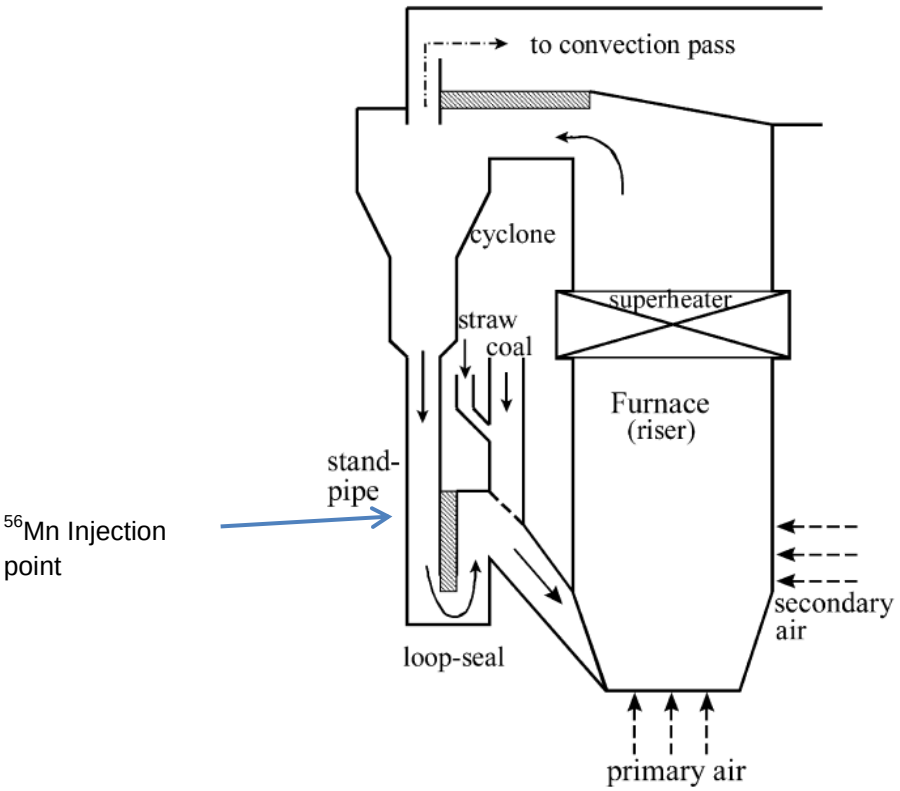

The signals from the two sets of detectors were collected by two data acquisition systems. Before each experiment, background radiation intensities were recorded, which were used later to correct the raw data.

A few grams of the dispensed tracer particles were injected into one of the standpipes by means of a probe using pressurized air. The results showed that the change of loading on the furnace has a significant effect on the mean residence time of particles in the dense and splash zones of the furnace.

8.4 Selection of radiotracers

In the CFB test, activated particles of magnesium containing alumina silicate were used to emulate the particles of fuel in the furnace. The selection of a suitable radioactive transmitter is crucial to the success of a radiotracer technique. For the same methodology to be deployed in a high-temperature aqueous environment, a

high-energy gamma-ray emitter is required that would be compatible with the aqueous, boiler feed system and which would not to lead to boiler material degradation. Therefore, the selection of a suitable tracer should ensure that:

- The physio-chemical properties should be consistent with those of the fluid being traced.
- The half-life of the tracer should be comparable to the duration of the test.

The IAEA (IAEA, 2009) used radiotracers in aqueous boiler systems and found that estimating the activity of radiotracer required for leak detection depends upon the:

- Volume flow rates of tube side and shell side, Q_t & Q_s respectively, measured in units of $m^3 s^{-1}$.
- Volumes of tube side and shell side, V_t & V_s respectively, (m^3).
- Detection efficiency of the leak detector at the outlet pipe, k (counts $s^{-1} Bq^{-1} m^3$)
- Minimum leak rate to be detected, $L_m = Q_1/Qs$ where Q_1 is the leak flow rate.
- Mixing characteristics of tube side and shell side.
- Accuracy of measurement.

Table 1 Common isotopes in use as radiotracers for leak detection (IAEA, 1995).

Radioisotope	Half Life	Gamma Energy	Chemical Form	Tracing Phase
Sodium-24	15 h	1.37 MeV	Sodium carbonate	Aqueous
Bromine-82	36 h	0.55 MeV 1.32 MeV	Ammonium bromide Methylbromide	Aqueous Gases
Iodine-131	8.04 d	0.36 MeV	Potassium or sodium iodide	Aqueous
Technetium-99m	6 h	0.14 MeV	Pertechnetate	Aqueous
Indium-113m	100 min	0.39 MeV	EDTA complex	Aqueous
Krypton-85	10.6 yr	0.51 MeV	Krypton	Gases
Krypton-79	35 h	0.51 MeV	Krypton	Gases
Xenon-133	5.27 d	0.081 MeV	Xenon	Gases
Argon-41	110 m	1.29 MeV	Argon	Gases

Table 2 common radiotracer isotopes in the aqueous phase, many are unsuitable to use in high temperature boilers due to their salt base.

Radioisotope	Half Life	Gamma Energy	Chemical Form	Reason for Unsuitability
Sodium-24	15 h	1.37 MeV	Sodium carbonate	Salt / relatively long ½ life
Bromine-82	36 h	0.55 MeV	Ammonium bromide	Acid salt / Long half-life
Iodine-131	8.04 d	0.36 MeV	Potassium or sodium iodide	Salt / ½ life / radiotoxicity / easily gets into food chain
Technetium-99m	6 h	0.14 meV	Pertechnetate	Salt/relatively long ½ life
Indium-113m	100 min	0.39 MeV	EDTA complex	Low Gamma Energy

8.5 An evaluation of Table 1 and 2 isotopes suitable for use in power plant heat recovery steam generators

The heat recovery steam generator in a CCGT has a water/steam high-pressure circuit and a high-temperature, low-pressure exhaust gas circuit that exhausts to atmosphere via a chimney stack.

Power plant heat recovery steam generators differ from closed-circuit tubed heat exchangers by the fact that the low-pressure gas side is exhausted to atmosphere via a discharge stack. Injection of a high-energy, long-lived radioactive isotope into the water side of the heat recovery steam generator would breach the circuit via any water/steam side leak or via the low-pressure gas side if the boiler tubes developed leaks.

Figure 20 HRSG exhaust flow route.

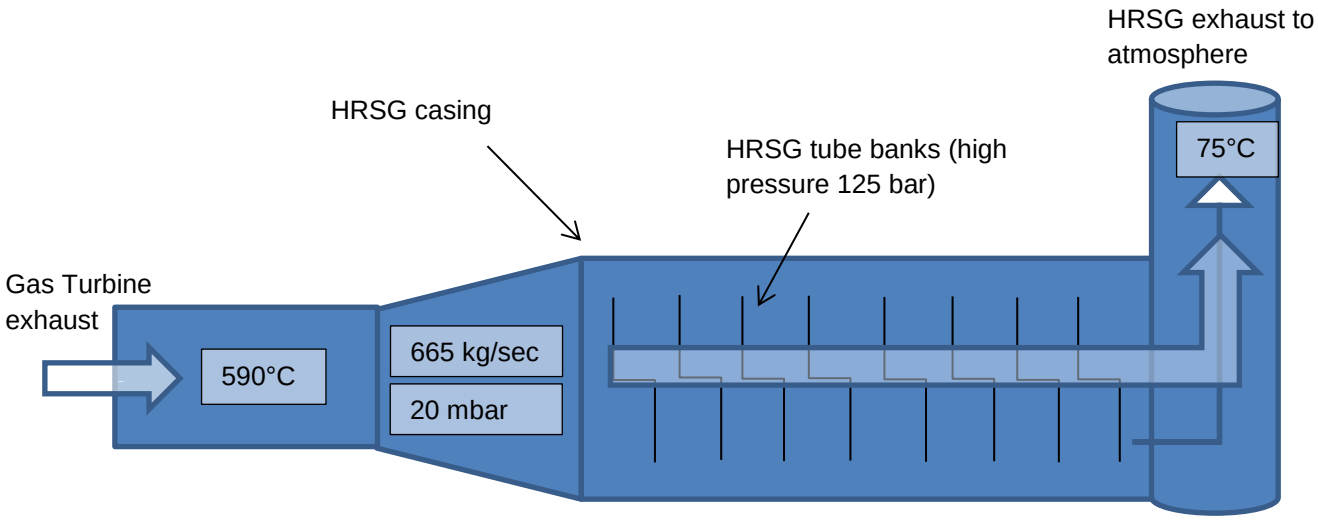

If the radionuclide passed from the closed circuit into the open circuit, low-pressure side via a leak site, it would be released to the environment via the HRSG exhaust stack. The longer the half-life of the radioisotope, the greater the exposure risk to the environment and to the people exposed to that environment.

In summary it is important that we consider the isotope half-life, its energy and its chemical form when selecting the correct isotope to inject into the heat recovery steam generator.

8.6 Potential release to the environment via the chimney, calculation of plume height

Isotopes that we inject into a boiler system will be carried via the leak site into the gas side of the boiler. The gas exits the boiler at high level (60m) via a chimney stack. The plume from the chimney is affected by atmospheric conditions and can form coning, looping, fanning, fumigation and lofting formations.

It is assumed that the structure of the plume is Gaussian in cross-wind and vertical directions.

The shape and behavior of the plume is important because the radioactive isotope injected into the boiler may be carried into the plume which later through dispersion reaches the ground.

Plume height and dispersion range from the stack depends on a number of factors, including: (Cushman-Roisin, 2012)

***F* = buoyancy flux (m^4/s^3)** Equation 1

g = 9.81 m/s^2

r = inner stack radius at tip (m)

W_s = fume vertical ejection velocity (m/s)

T_{air} = absolute temperature (K) at stack height

T_{fumes} absolute temperature of gas fumes (K)

$$F = gr2W\left(1 - \frac{Tair}{Tfumes}\right)$$ Equation 2

$$F = 9.81 * 9 * 5(1 - 288/348)$$

$F = 76\ m^4/s^3$

Then assuming a bent-over plume:

$$F < \frac{55m^4}{s^3}\ then\ xf = 49F^{5/8}$$ Equation 3

$$F \geq \frac{55m^4}{s^3}\ then\ xf = 119F^{\frac{2}{5}}$$ Equation 4

And therefore additional plume height (Δhb) above the chimney can be calculated (figure 21)

$$\Delta hb = 1.6\frac{F^{\frac{1}{3}}xf^{\frac{2}{3}}}{u}$$ Equation 5

Figure 21 Bent over plume distance over which plume rises (Cushman-Roisin, 2012).

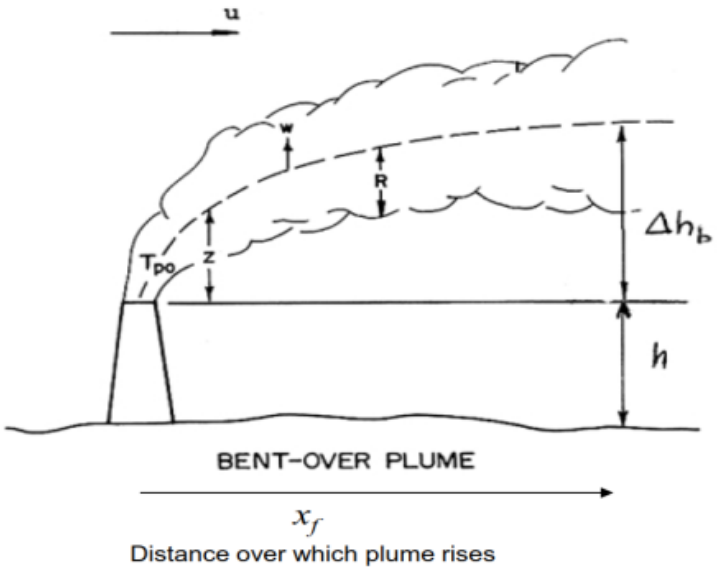

8.7 Radionuclides containing salts

The radiotracers that tend to be salt-based present a major problem in the operation of high temperature steam boilers due to the internal corrosion of boiler tubes. It is estimated that high-temperature, corrosion-related shutdowns account for 70% plant shutdowns (Bart et al, 2004).

Chlorides can cause superheater tube corrosion due to gaseous chloride attack and deposits containing chloride salts or a combination of molten chlorides and molten sulphates. They form deposits on the internal surfaces of the boiler tubes which interact with the metal oxide coating. The presence of chlorine prevents the formation of protective layers of oxide and causes accelerated attack in an oxidizing environment.

Chlorine can be in the form of hydrogen chloride (HCl), chlorine (Cl_2) or it can be combined with Na, K, Zn, Pb and Sn. Changes in temperature or the oxygen-chlorine ratio influences corrosion behavior. Active oxidation occurs above 450°C and this threshold temperature is exceeded in superheater and reheater tube passes where temperatures typically exceed 590°C.

Gases containing alkali chlorides (Nal and KCl) can cause direct corrosion by accelerating the oxidation of metal alloys. Volatized salt chlorides are deposited on the boiler tubes during cooling and affect corrosion by dissolving the oxide layer or by active oxidation. Wastage rates measured on waste to energy boilers are in the range of 1-3 mm/year for carbon steel.

Boiler corrosion experiments in waste-to-energy boilers found that the main driving factors in water-wall-tube attack are by the formation of low melting salt mixtures (Albina, 2005). Once the eutectic mixture is reached, the liquid phase on the surface of the metal increases the corrosion rate by faster chemical reaction and ionic charge transfer.

Figure 22 Influence of temperature on different corrosion mechanisms on boiler tubes (Albina, 2005).

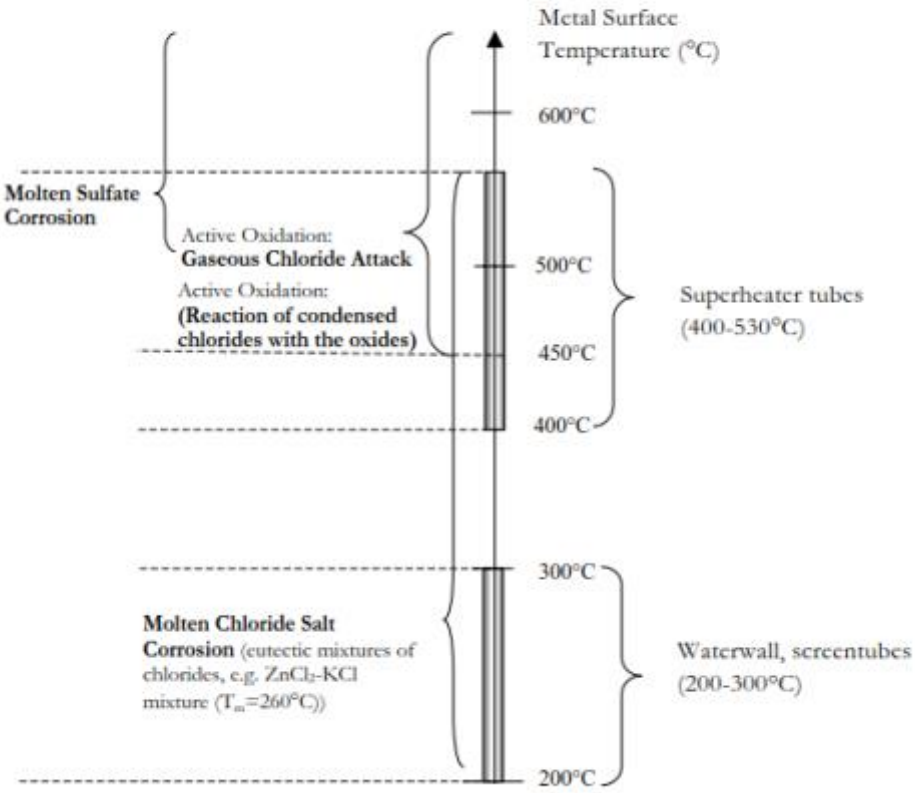

Therefore radiotracers that are predominantly salt or chloride-based will cause internal boiler corrosion and those with high-energy gamma-ray emissions and long half-lives can constitute a radiological hazard. Both are unsuitable for regular leak detection use in high-temperature steam boilers.

9 Radiotracers used in Positron Emission Tomography (PET)

PET is a nuclear medicine technique that uses radiopharmaceuticals in-vivo[4]. The radiation emitted, typically from an administered biochemical, is detected by a PET imager and a three-dimensional image of the distribution of the biochemical in the body is produced.

PET differs from other nuclear imagining techniques which exploit the emission of uncorrelated gamma rays by using positrons. Positrons undergo an annihilation reaction with an electron within 1-2 mm after being admitted to the body and in this reaction, two gamma rays are produced simultaneously, 180 degrees apart. The basis of PET detection is that when the gamma photons are emitted, a positron produced by the beta decay of the nucleus of the unstable tracer annihilates with an electron.

Figure 23 PET scanner scintillator arrangement with multiple PMT detector tubes (Scampini, n.d.).

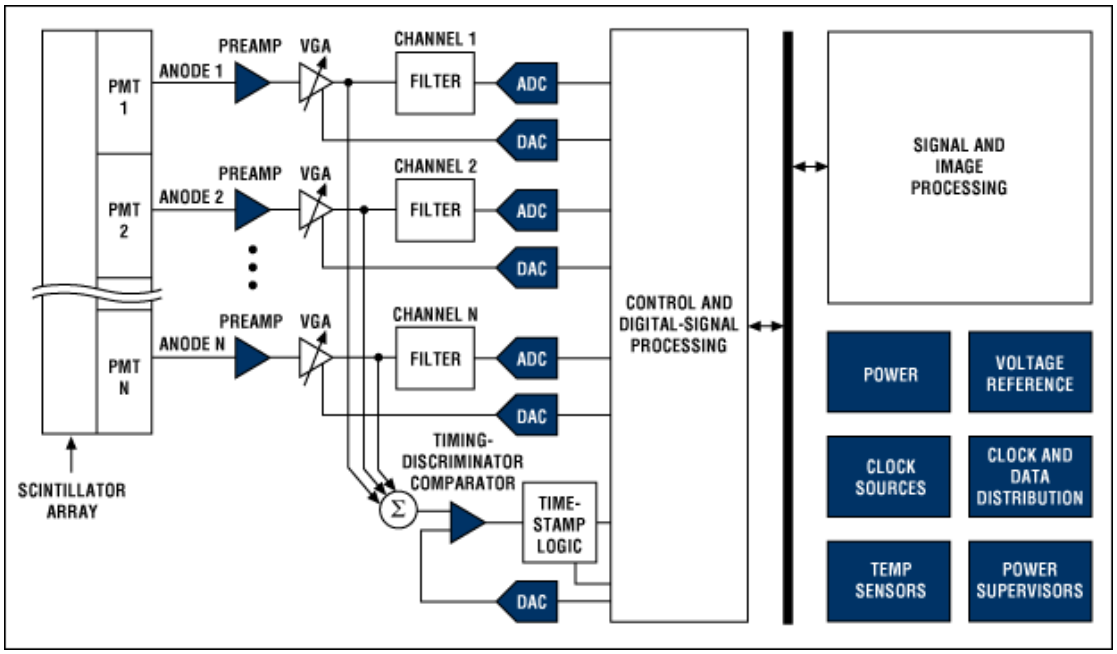

Detecting both photons simultaneously describes a line between the two associated detectors with the annihilation having occurred at some point along this line. The

[4] A process taking place in a living organism.

positron detectors are arranged typically in a ring and if two detectors register gamma rays at the same time, it is assumed that the annihilation took place along the line between the two detectors.

The detectors used for this application are typically sodium iodide doped with thallium (NaI(Tl)) scintillators, each coupled to a photomultiplier tube. Although a variety of other advanced scintillators have been developed specifically for the medical application of the technique. The positron-emitting substances most commonly used in PET techniques are isotopes of carbon, nitrogen, oxygen and fluorine. The isotopes are short-lived (2 minutes to 2 hours) and can be incorporated into chemicals suitable for injection in the body.

Table 3 commonly used radioisotopes for PET techniques.

Nuclide	$t_{½}$ life minutes	Decay mode	Max energy / MeV	Most probable energy / MeV
^{11}C	20.4	100% β^+	0.96	0.326
^{13}N	9.98	100% β^+	1.19	0.432
^{15}O	2.03	100% β^+	1.7	0.650
^{18}F	109.8	97% β^+/3%EC	0.69	0.202

- ^{11}C - molecule most stable in an oxidizing environment is CO_2, in a reducing environment CH_4. It is a cyclotron produced radionuclide; ^{11}C choline is produced and available in a sodium chloride solution.
- ^{13}N - N_2 in the gas phase and NO_{3-} in aqueous solution.
- ^{15}O - O_2 gas, in aqueous solutions the precursor is water.
- ^{18}F – fluorine gas F_2

^{13}N-labelled precursors may be interesting as they can be incorporated into ammonia which is already injected into the boiler feed water to raise the pH for corrosion prevention issues.

9.1.1 Relevance of PET isotopes

The relevance and applicability of the commonly used PET isotopes in this study lies in their high energy, short half-life characteristics. The heat recovery steam generators used in gas turbine combined cycle power plants have an exhaust stack that is open to atmosphere. Emission of any long half-life radionuclide with the exhaust gases would present a radiation hazard in the stack gas fall out area and potentially contaminating boiler structures and surfaces.

Ideally, the radioactive residence time in the boiler system should be long enough to complete a circuit of the boiler system without the isotope becoming a radiological hazard to the operators of the plant.

10 Selection of the most suitable radioisotope and the evaluation of ^{13}N

^{13}N used for PET applications is produced in the form of $^{13}NH_3$. This radiotracer has potential for use in power station boiler feedwater systems due to its compatibility for injection into the boiler stream. It emits gamma (γ) radiation at an energy of 511 keV and because it has a short half-life (~10 minutes).

One of the selection criteria of a suitable radiotracer is that the radiotracer's physio-chemical nature should be compatible with the fluid being traced. If $^{13}NH_3$ is a suitable radiotracer to be injected into the boiler feedwater, then we need to evaluate the physio-chemical characteristics that the radiotracer will be subjected to in a power station boiler.

Boiler feedwater is dosed with ammonia (NH_3) to limit the effects of corrosion on the internal boiler components, as mentioned above. The boiler feedwater is maintained

at greater than 9.6 pH using a 20% NH_3 aqueous solution. This is injected into the feedwater by a positive displacement pump. The fraction of NH_3 or NH_4^+ that the feedwater contains is temperature-dependent: at a pH of 9.2 and a temperature of 25°C, ammonia and ammonium co-exist equally.

The feedwater pH is maintained >9.6 for corrosion protection and at the ammonia injection point, the water temperature is ~ 25°C. As the feedwater is pumped into the pre-heater and economizer sections of the boiler, the feedwater temperature increases and therefore the fraction of NH_4^+ decreases until at >75°C and with a pH >9.6, only NH_3 exists.

Typical boiler section temperatures for a CCGT are:

- LP Preheater 146°C
- IP Superheater 240°C
- IP Reheater 552°C
- HP Superheater 480°C
- HP Final Attemperator 555°C.

Figure 24 relationship between temperature, pH and NH_4^+ fraction. (Long, 2012)

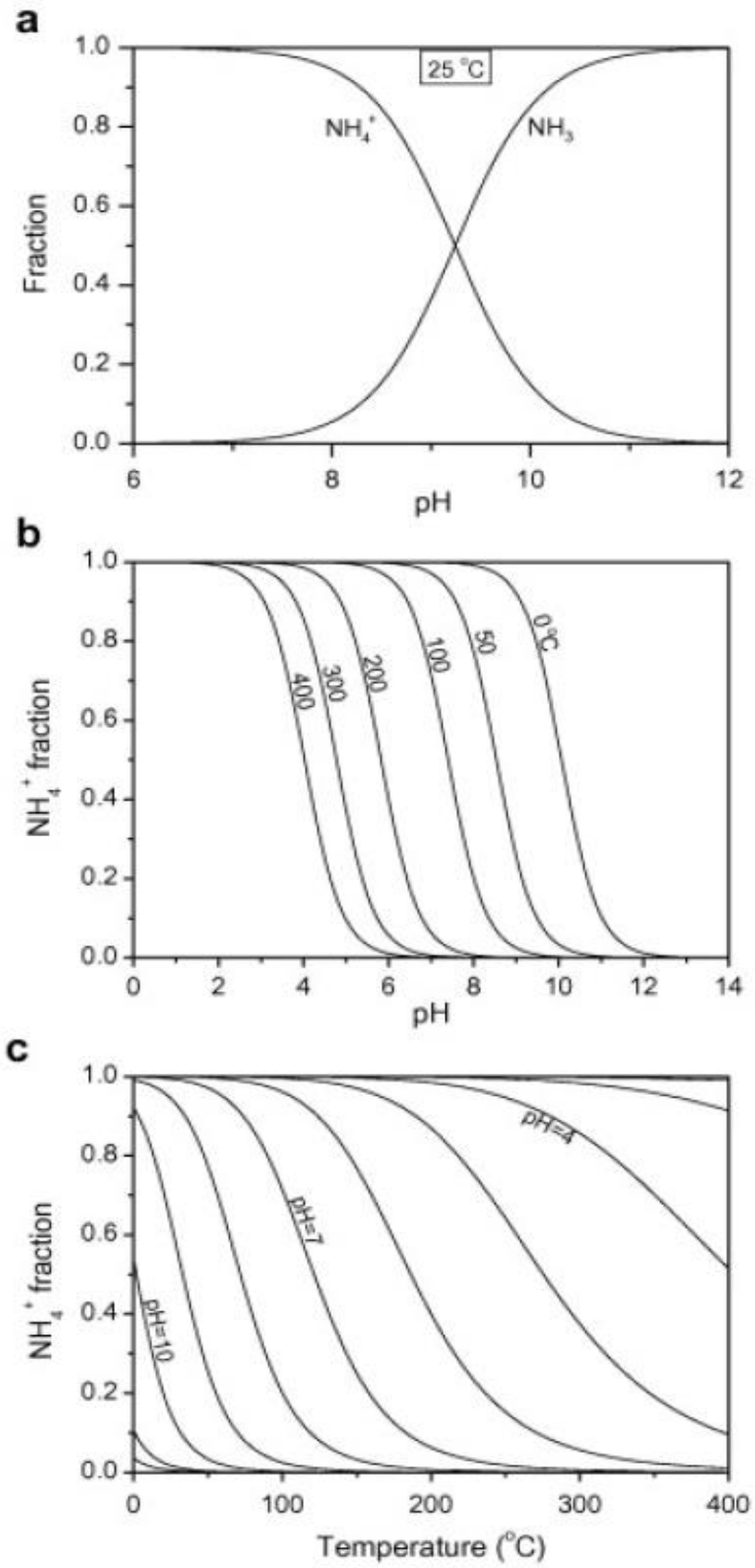

The stability of ammonium is strongly dependent on pH and temperature, with the equilibrium equation being:

$$NH_4^+ + OH^- \overset{Ka}{\Leftrightarrow} NH_3(aq) + H_2O$$ **Equation 6**

Where the temperature-dependent equilibrium constant is given by:

$$pKa = \frac{2533}{T} - 0.5936\ lnT + 4.127$$ (as determined by Olofsson 1975) **Equation 7**

Where in Figure 24 relationship between temperature, pH and NH_4^+ fraction. (a) shows that the aqueous reduced nitrogen species at 25°C is mainly ammonium when pH is lower than 7 and ammonia when pH is higher than 11.5

And in Figure 24 relationship between temperature, pH and NH_4^+ fraction. (b) ammonium fractions change with pH for temperatures from 0 to 400 °C, indicating that ammonium destabilizes at lower pH when temperature is higher.

And in Figure 24 relationship between temperature, pH and NH_4^+ fraction. (c) ammonium fractions change with temperature for pH from 2 to 11.

10.1 Production of PET Radiotracers using an 11 MeV medical cyclotron

^{13}N is a cyclotron-produced radionuclide via the ^{16}O (p, α) ^{13}N reaction with 11 MeV protons. The production of radionuclides with an accelerator requires that particle beams are delivered with two specific characteristics: The beams must have sufficient energy to bring about the required nuclear reactions and have sufficient beam current to give satisfactory yields in adequate timescales.

Liquid targets are the most popular method used to produce ^{13}N. The most-widely used targets are water targets and water targets with added ethanol. The basic characteristics of all cyclotrons are similar: there is an ion source to produce ions, an acceleration chamber to accelerate them and a magnet to contain the ions on a circular path.

10.1.1 Nuclear reactions

As a charged particle passes through a material with sufficient energy to interact with the nucleus of an atom, it will either interact with a nucleus or be scattered. If there is sufficient energy it might form a compound nucleus that might subsequently disintegrate to produce a different nucleus. The incident particle must have sufficient energy to overcome a barrier known as the electrostatic barrier or Coulomb barrier, the height of which corresponds to the *Q* value or mass difference between the sum of the incoming particle and the target nucleus and that of the resultant nucleus and any reaction products

10.1.2 Coulomb barrier

The production of radio-nuclides with a cyclotron requires that the charged particle must have energy greater than the electrostatic repulsion between the incident particle and the target nuclide.

10.1.3 *Q* value

The total energy including the mass of the reaction constituents must be equal to the total energy including the mass of the products. Any increase in kinetic energy by the incoming particle must be accompanied by a decrease in the mass.

The *Q* value of a nuclear reaction may be either positive or negative. If the rest masses of the reactants exceed the rest masses of the products, the *Q* value of the reaction is positive, with the decrease in rest mass being converted into a gain in kinetic energy.

If $Q < 0$ the reaction is termed endoergic: the energy supplied must be greater than the Coulomb barrier in order for the reaction to proceed.

If $Q > 0$ the reaction is said to be exoergic, the threshold energy is the height of the Coulomb barrier.

Figure 25 Q values and thresholds for the reaction of a deuteron with a ^{14}N nucleus forming a compound ^{16}O (IAEA, 2009).

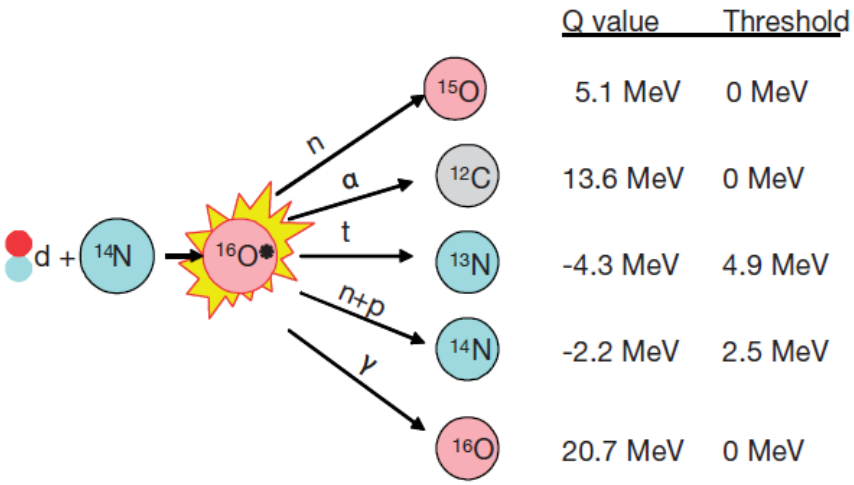

The cyclotron target is introduced into the beam where under irradiation, the new radionuclide is produced.

Figure 26 Cyclotron and canister for target isotope (IAEA, 2009).

11 Instrumentation suitable for detecting 511 keV gamma rays

It is postulated that the instrumentation for detecting ^{13}N would be located at the stack outlet where most of the plant environmental monitoring equipment is located. The stack outlet instrumentation for monitoring carbon monoxide and nitrous oxides is located on a platform at the 65 m level of a typical CCGT stack.

Figure 27 sampling stack platform and ports.

A literature review to determine if detectors are available commercially for detecting ^{13}N carried out in this project revealed that sampling of the containment atmosphere for ^{13}N is a requirement of the Westinghouse AP1000 design pressurized water reactor. (NRC, 2011)

In the AP1000, the containment atmosphere radiation monitor measures the radioactive gas concentrations associated with ^{13}N and ^{18}F in the containment atmosphere. The containment atmosphere radiation monitor is a part of the reactor coolant pressure boundary leak detection system. The presence of gaseous radioactivity in the containment atmosphere is an indication of reactor coolant pressure boundary leakage.

The containment atmosphere radiation monitor accepts analog signal inputs for sample flow and temperature. These signals are used to calculate concentrations at standard conditions. The $^{13}N/^{18}F$ detector is a gamma-sensitive, thallium-activated, sodium iodide scintillation detector with a window at 511 keV.

11.1 Evaluation of cerium-doped lutetium orthosilicate (LSO) with bismuth germinate and thallium doped sodium iodide

Typical detectors suitable for 511 keV gamma rays have been thallium-doped sodium iodide NaI(Tl) coupled to photomultiplier tubes (PMTs). With the relatively recent discovery of bismuth germinate $Bi_4GE_3O_{12}$ (BGO) and lutetium orthosilicate Lu_2SiO_5 (CE) (LSO), most detector applications were converted to these materials because of higher detection efficiencies for gamma rays.

The block arrangement has become the design used most widely, comprising typically 64 elements connected to 4 PMTs.

$Bi_4GE_3O_{12}$ and LSO scintillators have several advantages over NaI(Tl). They have a higher density (~7 g/cm^3 as opposed to ~3.7 g/cm^3 for NaI(Tl)) providing more efficient detection. They are non-hygroscopic and are rugged, i.e. not as fragile as sodium iodide, allowing simple construction.

NaI(Tl) detectors have low efficiencies for gamma rays with energies over 200 keV because of a material density with respect to atomic number Z that is low relative to the more recently-discovered alternatives. Since the use of ^{13}N which results in the emission of a pair of 511 keV gamma rays, detection efficiencies are can be low unless relatively large detectors are used.

BGO has a relatively long decay constant of 300 ns which limits its count rate. LSO has a decay constant of 40 ns and therefore exhibits good count rate and high light output.

Gamma rays interact with matter in the energy region of interest to this research via the photoelectric effect and the Compton Effect. In the former, the gamma ray is adsorbed by an atom that ejects an electron producing the characteristic x–ray resulting in the full energy of the gamma ray being absorbed. In Compton scattering,

the gamma ray loses a fraction of the energy to an electron through scattering. The electron energy is absorbed in the crystal; scattered gamma rays that are not absorbed are lost from the detector.

If the linear attenuation coefficients for NaI(Tl), BGO and LSO are compared above 100 keV energies, the advantages become clear, NaI(Tl) detectors must be twice as thick to achieve similar efficiencies.

Photomultipliers with glass windows have a maximum sensitivity near to 400 nm, it is advantageous for the scintillator to have its emission maximum near this wavelength. Both NaI(Tl) and LSO have intense emissions that peak near 400 nm, however BGO peaks at around 480 nm. The intensity of the emission affects the number of crystal elements that can be coupled to a single PMT; reducing the number of PMTs required generates a substantial cost saving. For example, BGO: 16 crystals per PMT, for LSO: 144 crystals per PMT.

Figure 28 Bismuth Germinate detector block and photomultiplier tubes (UC San Diego school of medicine, 2018).

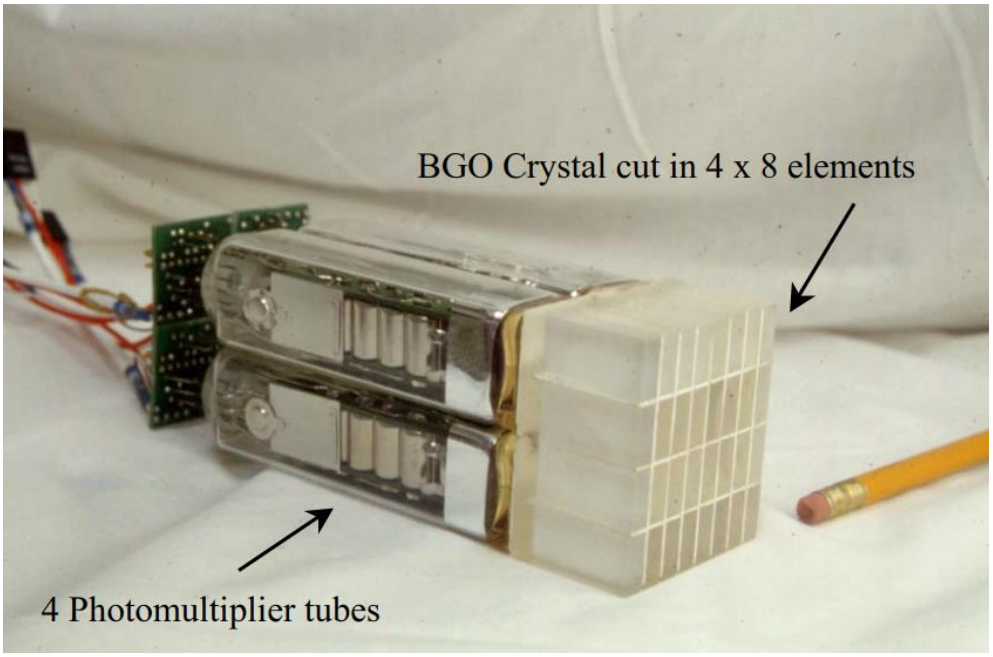

Figure 29 Bismuth Germinate detector operation (UC San Diego school of medicine, 2018).

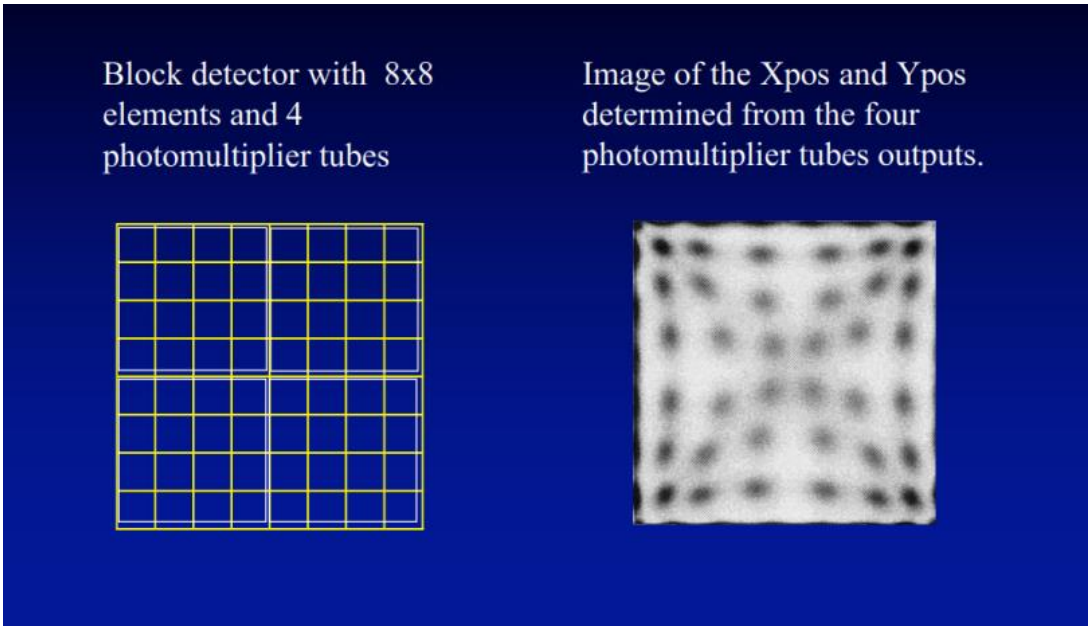

12 Radioactivity plate out in boilers

Heat recovery steam generators, of the type used with large industrial gas turbines, incorporate multiple passes of heating elements (tube banks). The heating elements produce process steam for consumption in a steam turbine.

Boiler inlet gas temperatures of 590°C are reduced typically to 75°C at the boiler outlet (economizer) section of the boiler. Final boiler exit temperatures are closely controlled to ensure that the dew point is not reached which can otherwise result in the formation of sulfuric acid on boiler components. The natural gas composition is monitored for sulphur content and the exhaust temperatures are adjusted accordingly.

It is unknown if the radioactive tracer emitted from a boiler leak site would plate-out on the colder surfaces of the boiler before it could be detected by the monitoring system installed at the top of a 65 m stack.

Evaluation of boiler plate-out, that is, radioactive plate out on the boiler surfaces, has been researched within the nuclear industry for reactor fission products in the chemical form of ^{131}I and ^{137}Cs.

The Korean Atomic Research Institute (Korean Atomic Research Institute, 2009) analysed fission product transport mechanisms and plate-out behaviour in a gas-cooled Very High Temperature Reactor (VHTR) design. Applications to determine the major factors contributing to the overall uncertainties in predicting the plate-out phenomena in reactors are limited. Plate-out phenomena have been an important safety issue for gas-cooled reactors but there is at present no suitable analysis tool that can be applied in modelling safety cases.

12.1 Aerosol boiler plate-out

Boiler plate-out is the accumulation of atoms or molecules onto the surface of the adsorbents by either chemical or physical attraction (adsorption). The plate-out mechanism is thought to be the dominant removal mechanism for the condensable fission products in a gas reactor (IAEA, 1995).

The Symptom Based Emergency Response Guidelines (SBERGS) and Severe Accident Guidelines (SAG's) for Advanced Gas-cooled Reactors (AGRs) recognizes that boiler plate-out is advantageous during post fault recovery of a reactor that is depressurizing due to a severe fault condition. The emergency feed system draws boiler feed water from feedwater tanks maintained at 25°C, the relatively cold emergency feed system is designed to maximize fission product plate-out on the boiler surfaces instead of being released to the atmosphere via the leak site.

Figure 30 Fission product transport and plate out.

Three regions were modelled;

1. Bulk coolant
2. Thin boundary layer
3. Structural Surface

Where;

***K*:** Species

C: Bulk concentration in the coolant [m^{-3}]

S: Surface contamination [m^{-2}]

B: Concentration within boundary layer [m^{-3}]

λ: Decay constant [s^{-1}]

h: Mass transfer coefficients [m s^{-1}]

q_c: Volumeric flow rate [m^{-3} s^{-1}]

Qs: Surface source rate [m^{-2} s^{-1}]

D: Difusion coefficient [m^{-2} s^{-1}]

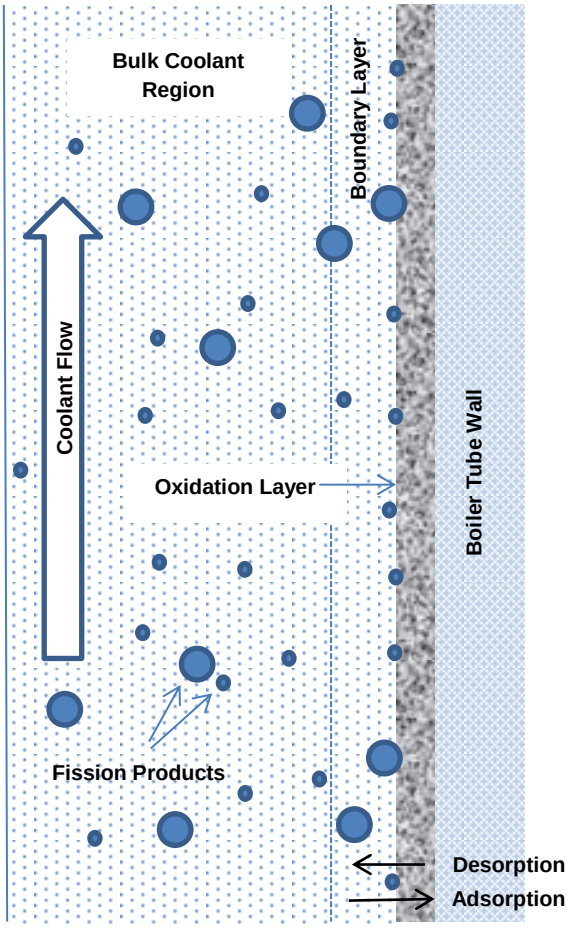

B_K (surface concentration of species) can be evaluated using ideal gas law. This provides a significant insight into predicting fission product behavior near the surface of the components.

The Korean Atomic Research Institute analysed fission product transport mechanisms and plate-out behaviour in a gas cooled Very High Temperature Reactor (VHTR) (Sang-Baik, 2009). A hot-gas sampling tube was installed inside the reactor to identify the deposition and diffusion profiles along the titanium (Ti) and chrome molybdenum (Cr-Mo) sampling tube.

Two meaningful factors on the plate-out phenomena were found through sensitivity analysis from the VHTR research.

- The ***Diffusion coefficient*** was found to play an important role in predicting the adsorption of ^{131}I and ^{137}Cs.
- The ***Surface conditions*** of the coolant circuit can also be major source of the uncertainty in the prediction of the plate-out activity of ^{131}I.

It was also found that plate out is dominant over the lower temperature region for I-131 however the higher temperature oxide layers prevented ^{131}I formation.

Thus, the impacts from the surface oxidation condition as well as the diffusion coefficient have to be quantified in the prediction of the fission product plate-out for every tracer postulated to be of use.

The model used by the Korean Atomic Research Institute (MELCOR) to simulate the fission product plate out was found to not accurately predict the plate out of ^{131}I over the test surface and only predict plate-out of ^{137}Cs at low temperatures.

The influencing parameters for plate out were found to be:

- Fission product release rate,
- Gas velocity,
- Degree of nodalization of the circuit (as opposed to dispersion),
- Lennard-Jones parameter values (a mathematical model that simulates the interaction between molecules,
- Chemical form of the isotopes.

12.2 Modelling the internal gas flow in a heat recovery steam generator

Power plant boilers are designed with high Reynolds[5] numbers to ensure that homogeneous mixing occurs and that heat is transferred uniformly across the boiler structure. Modelling the internal gas flow in a full-size heat recovery steam generator would require the boiler spaces to be fully instrumented.

In order to understand the dynamics involved, a simple air box was manufactured to simulate gas flow through a boiler space.

A simple airflow model was constructed in this research using medium-density fibreboard (MDF) and a 100 mm diameter extraction fan to provide airflow through the box. Airflow indicators were placed at suitable locations to determine airflow inside the box and around the installed baffles. The box lid was cut out and an acrylic viewing window inserted to observe the airflow direction from the installed indicators.

Figure 31 postulated direction of airflow indicators.

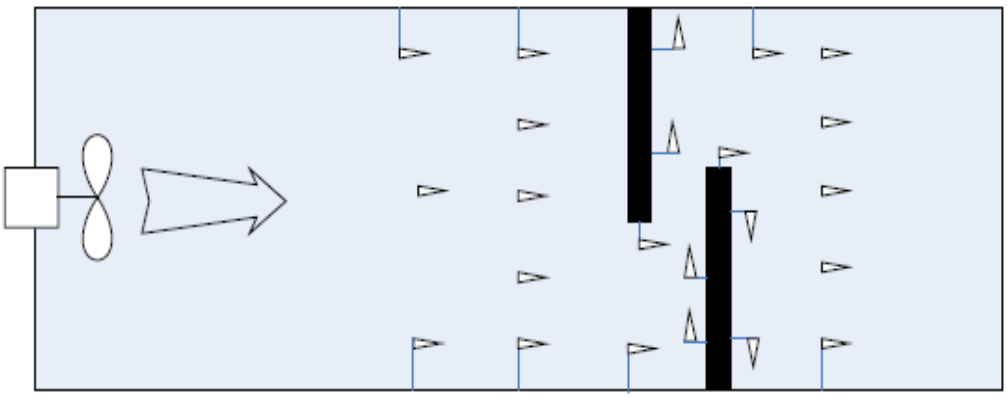

Flags indicating direction of flow around baffle plates

[5] Reynolds number - is a dimensionless value that measures the ratio of inertial forces to viscous forces and describes the degree of laminar or turbulent flow.

Airflow mapping in an environment can be carried out using Naïve physics algorithm (NaReM) and using this airflow map; it is reasoned that radioactive dispersal will follow the air flow dispersal (Russell, 2006). Naïve physics is one method of airflow modelling as it avoids some of the difficulties encountered using computerized fluid dynamics.

There are three major sources of uncertainty:

1. Uncertainty of the physical map. The map provided may be imprecise.
2. Unknown boundary conditions**.** Direction of airflow through a duct may be unknown, this is a significant effect.
3. Formation of distinct stable airflow patterns. The airflow against a solid surface can be accounted for but airflow at decision boundaries are more difficult, i.e. where more than one course of action could occur such as when airflow meets an object in its path where there are multiple choices as in the figure below.

Figure 32 Airflow around obstacles (Russell, 2006).

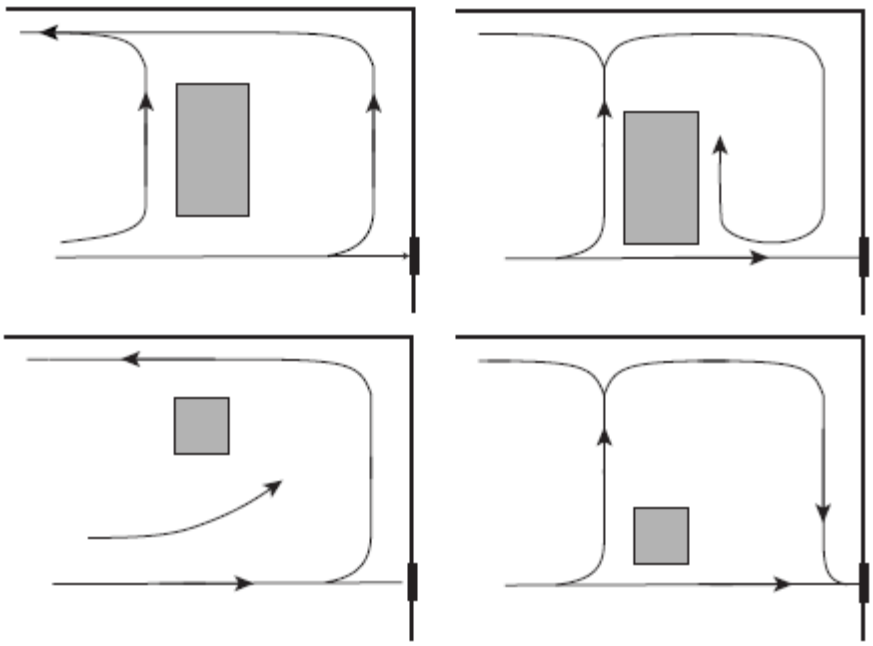

Airflow moves out laterally as it advances, the algorithm traces flows in layers, inlet flow is propagated as a discrete flow until it is complete, then further layers are initiated around the flow simulating the spreading of flow laterally.

Flow past obstacles

The scenario from Figure 32 Airflow around obstacles.shows that a variety of flow patterns arose when Russell and Kowadlo of Monash University Australia (Kowadlo, 2012) tried to predict flow patterns around objects. This was verified by them using Flo++ and verified through practical their practical experimentation. Significantly different stable macroscopic flow patterns occurred with small changes in the vertical position of each of the obstructions.

Figure 33 Air box construction to demonstrate air flow past obstacles.

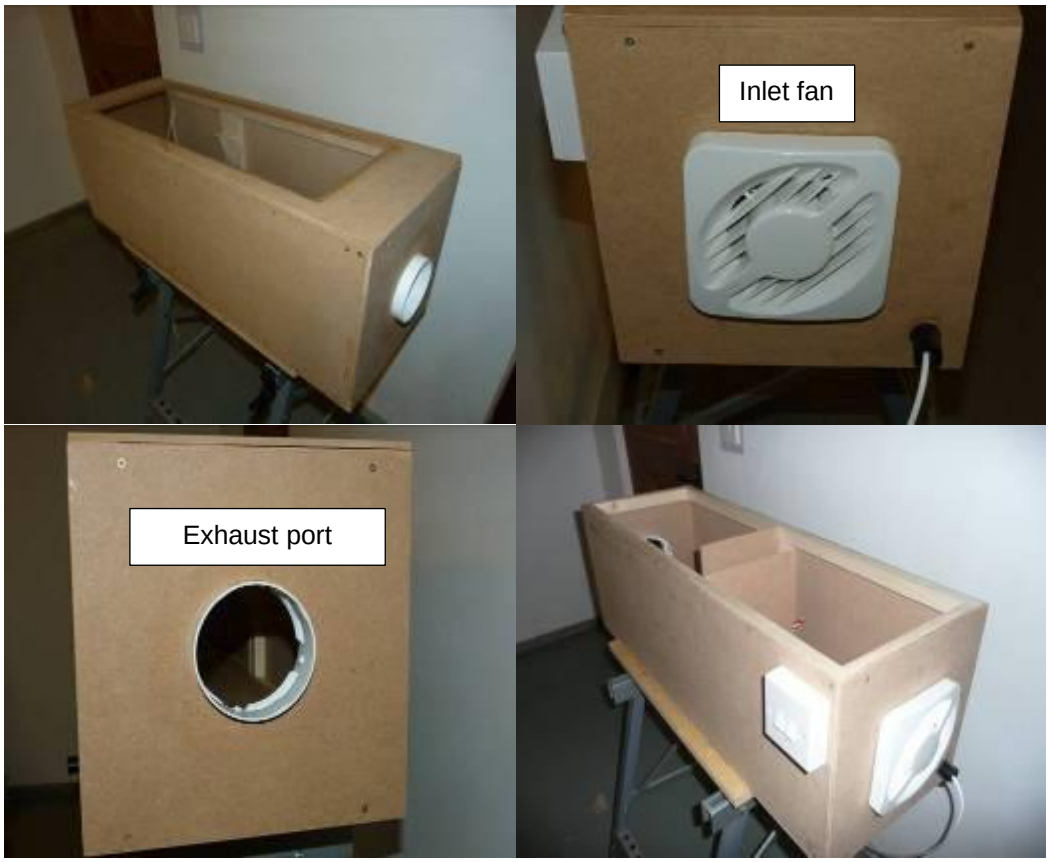

12.2.1 One baffle fitted showing direction of airflow around it.

Airflow indicators were fitted to the demonstrator to extract flow dynamics. The indicators show airflow is significant at the decision boundary of the baffle edge. At the rear of the baffle it is possible that airflow eddies upwards before turning down to join the main airflow to the exit.

Figure 34 Airflow directional paths around one baffle.

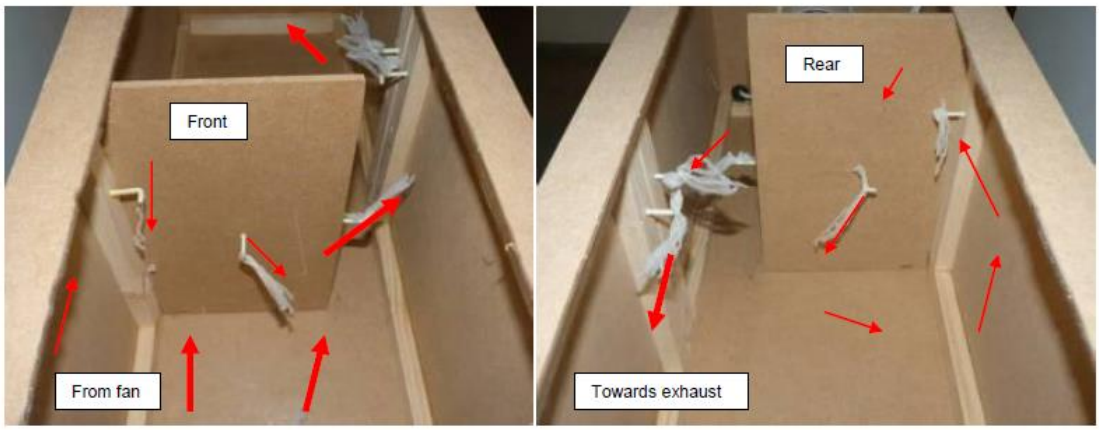

12.3 Two baffles fitted showing direction of airflow around them.

With both baffles installed the airflow from the leading edge of the first baffle impacts the second baffle plate. This directs the airflow towards the box edge, and significant flow is observed at the edge of the second baffle before exiting the box.

Figure 35 Airflow directional paths around two baffles.

12.3.1 Discussion of the findings

From the manufacturer's literature, the 100 mm diameter fan generated approximately 80 m^3/hr (22.2 l/s & 2.74 m/s) air flow. This was barely enough to lift the indicators, for further testing it was decided to increase the flow rate of the fan. The duct size was 300 mm x 300 mm: hence using the 80 m3/hr fan would equate to a 0.25 m/s airflow speed in the duct. The airflow speed around the baffles, where the duct size narrows to 300 mm x 100 mm, increased to 0.75 m/s. The airflow indicators demonstrate the increased speed around the baffles. This observation repeats what has been identified in the review of airflow mapping, i.e. that the airflow must be of sufficient strength to be sensed reliably.

12.3.2 Repeat test with airflow box fitted with up-rated fan

An uprated fan was fitted to increase airflow to 550 m^3/hr. The following calculations were obtained during the test:

- Mass flow rate through the box was calculated to be 0.195 kg/s
- Velocity through box 1.7 m/s
- Velocity around baffles 5.1 m/s
- Exit velocity from 100 mm outlet 19.49 m/s

Figure 36 Air box model fitted with an uprated fan to increase airflow.

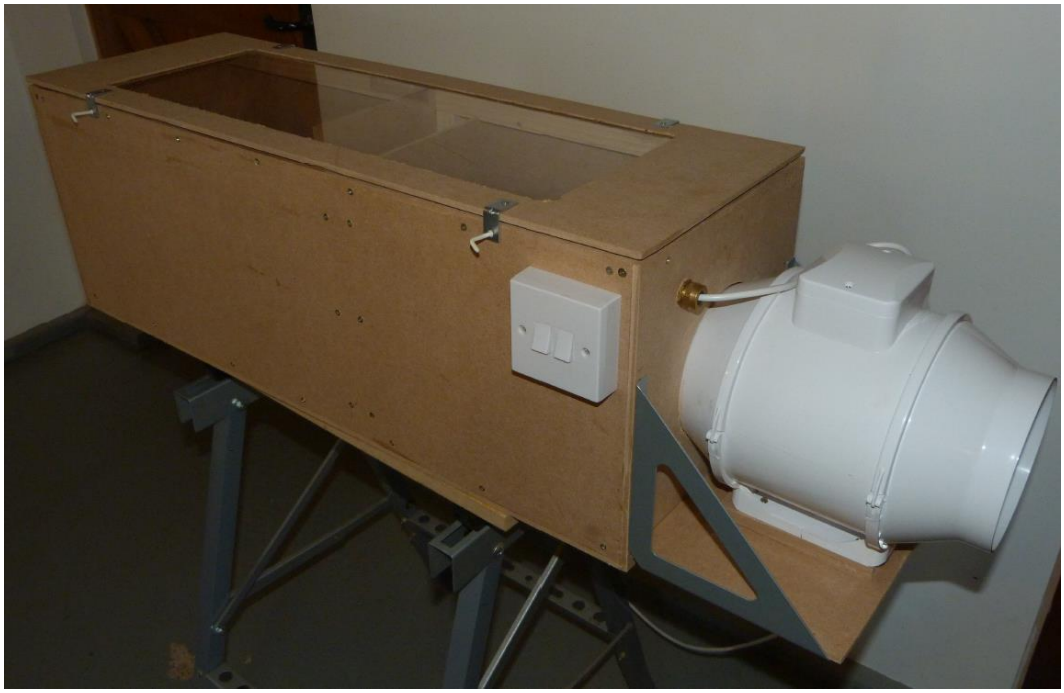

Figure 37 Airflow telltale directions using the uprated fan.

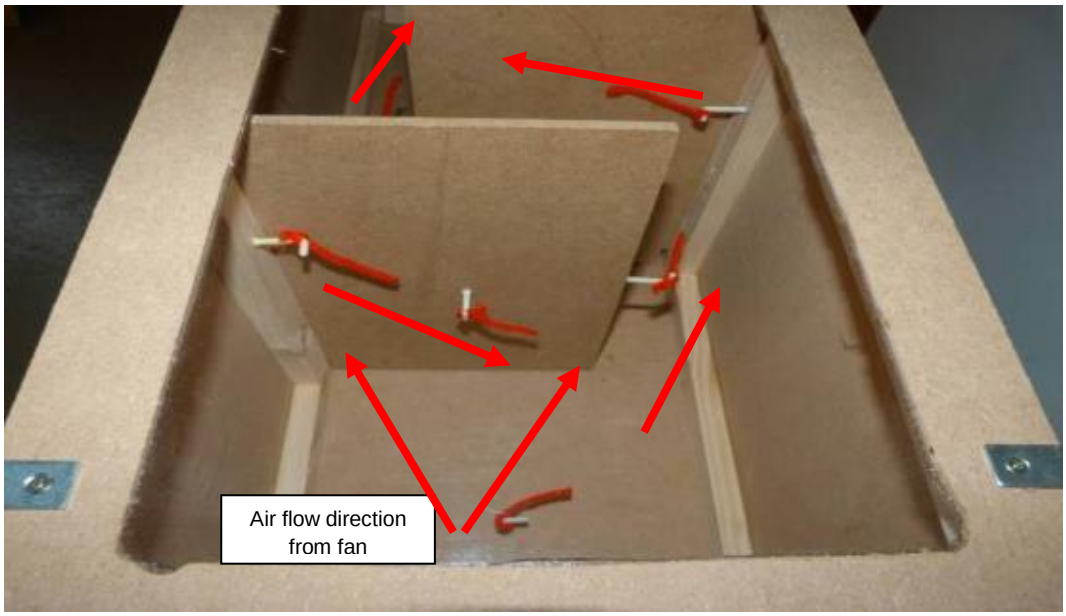

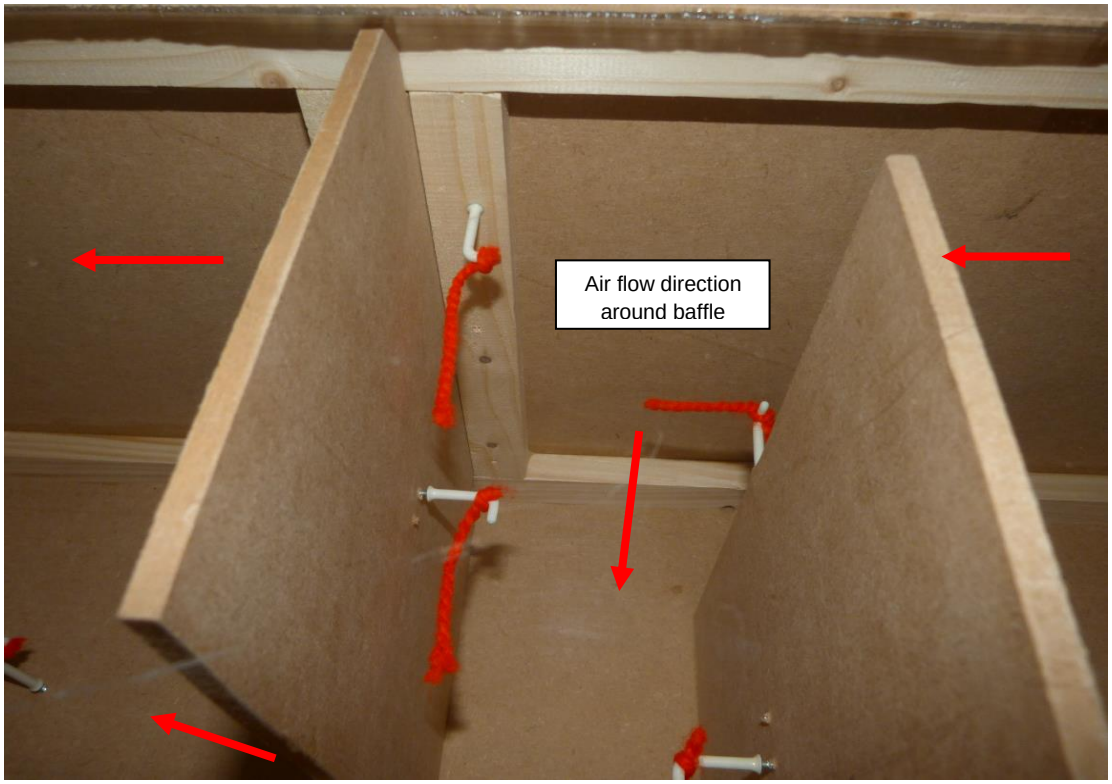

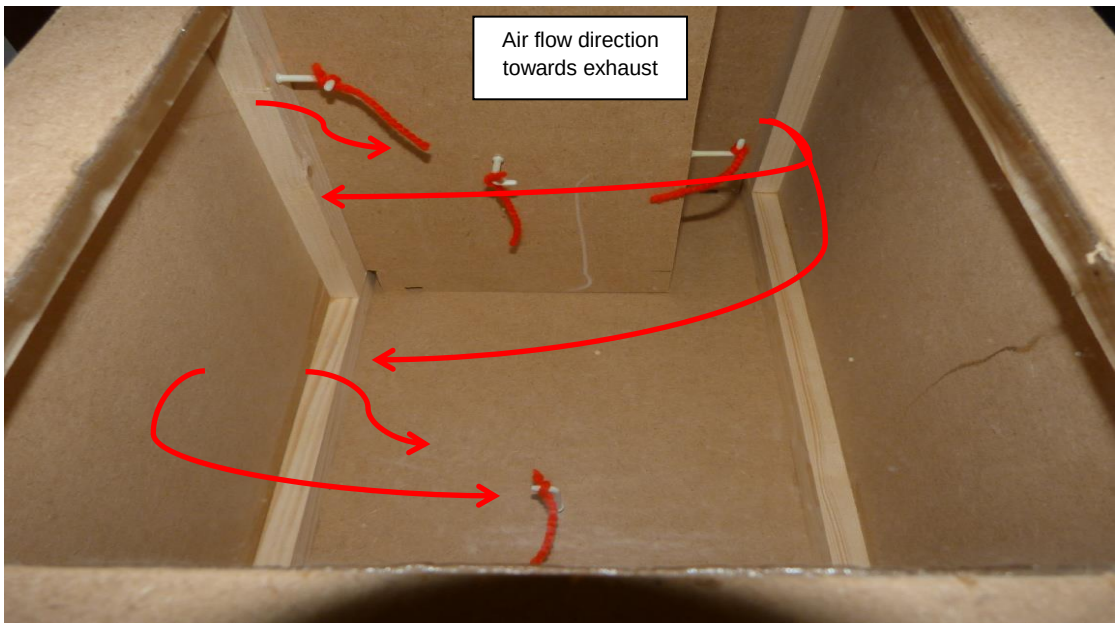

12.4 Air box model calculations

Volume flow rate **= m^3/s =** Mass flow rate **kg/s** / Density of air ρ **kg/m^3** Equation 8

Mass flow rate **kg/s =** Volume flow rate **m^3/s *** ρ Equation 9

And if density of dry air **ρ** = 1.275 kg/m^3 at 15°C

Then; Mass flow rate through the airbox = 550 m^3/hr * 1.275 kg/m^3 / 3600 = 0.195 kg/s

Area of model = 0.3 m * 0.3 m = 0.09 m^2

And if Speed = Volume Flow Rate / Flow Area Equation 10

Then speed through box at 550 m^3/hr = 0.153 m^3/s / 0.09 m^2 = 1.7 m/s

And if area through baffles = 0.3 m * 0.1 m = 0.03 m^2

Then speed through baffled area = 0.153 m^3/s / 0.03 = 5.1 m/s

If air box exit = 100 mm diameter tube

Then Exit Speed from model = Volume Flow Rate / Flow Area

Flow area = π R^2 Equation 11

So π * 0.05^2 = 0.00785 m^2

153m^3/s / 0.00785m^2 = 19.49 m/s

Gas Turbine and Boiler calculations

Typical Gas Turbine Mass flow at exhaust for Siemens 4000F machine is ~ 650 kg/s at base load

Volume flow rate = MFR / ρ Equation 12

If ρ of dry air at 15°C then 15°C + 275K = 288K

Then if GT exhaust temp = 595°C + 275K = 870K

So 288 / 870 * 1.275 = 0.4221 kg/m^3

ρ of dry air at 595°C = 0.4221 kg/m^3

So VFR = 650 kg/s / 0.4421 kg/m^3 = 1540 m^3/s

And if boiler area = 21.716 m * 11.007 m = 239.3 m^2

Then Speed = Volume Flow Rate / Flow Area Equation 13

Then 650 m^3/hr = 1540 m^3/s / 239.3 m^2 = 6.44 m/s

If boiler exit = 8.0 m diameter stack

Then exit speed = Volume Flow Rate / Flow Area

Flow area = π R^2

So π * 4^2 = 50.27 m^2

1540 / 50.27 = 30.63 m/s

Exit speed from stack= 30.63 m/s

Table 4 Comparison of volume flow rates, mass flow rates and velocities through air box and Gas Turbine.

Parameter	Air box model	Gas Turbine & Boiler
Volume flow rate **m^3/s (supply)**	0.153 m^3/s	1540 m^3/s
Mass flow rates **kg/s**	0.195 kg/s	650 kg/s
Speed through system **m/s**	1.7 m/s	6.44 m/s
Speed at exit **m/s**	19.49 m/s	30.63 m/s

12.4.1 Scaling Factor of CCGT boiler relative to the air box:

Cross Sectional Areas

Boiler = 239.3 m^2

Airbox = 0.09 m^2

Flows

Boiler = 1540 m^3/s

Airbox = 0.153 m^3/s

Scaling Factor[6] – (flow rate per unit area)

Boiler 1540 m^3/s / 239.3 m^2 = 6.44

Airbox 0.153 m^3/s / 0.09 m^2 = 1.7

12.5 Measuring Airflow

12.5.1 Pitot tube

The volumetric airflow can be determined by measuring the speed of the air as it passes through the known diameter of the Pitot tube. The low speed of air through the air box (1.7 m/s) is at the very lower end of the range the Pitot tube could measure and this would lead to related systematic inaccuracies in the measurements obtained.

Figure 38 Thin film thermal mass air flow sensor used to detect airflow pressures in test box. (Freescale Semiconductor, 2012)

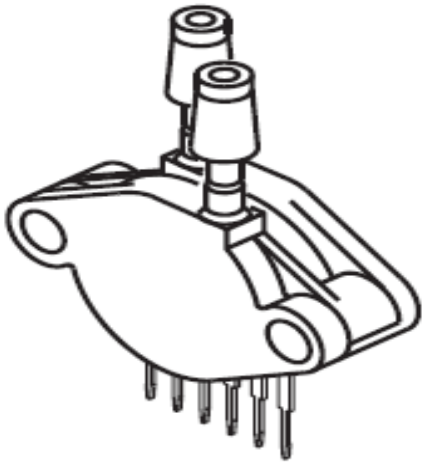

A piezo-resistive transducer monolithic silicon pressure sensor was used to provide an analogue output signal that is proportional to the applied pressure (range 0 to 50 kPa). The pressure side (P1) was routed to the measurement position by 4 mm silicon tubing, the vacuum side (P2) was routed outside the air box.

[6] Assuming a direct relationship for the scaling factor. Practically the boiler and air box will have different Reynolds numbers; the turbulence in the boiler will be greater. Boilers typically have baffle plates to direct combustion gas flows to specific areas which generate local environments not modelled here.

The transducers were mounted on a solderless breadboard and connected to a 5V DC power supply.

Figure 39 Air flow transducers fitted to a breadboard.

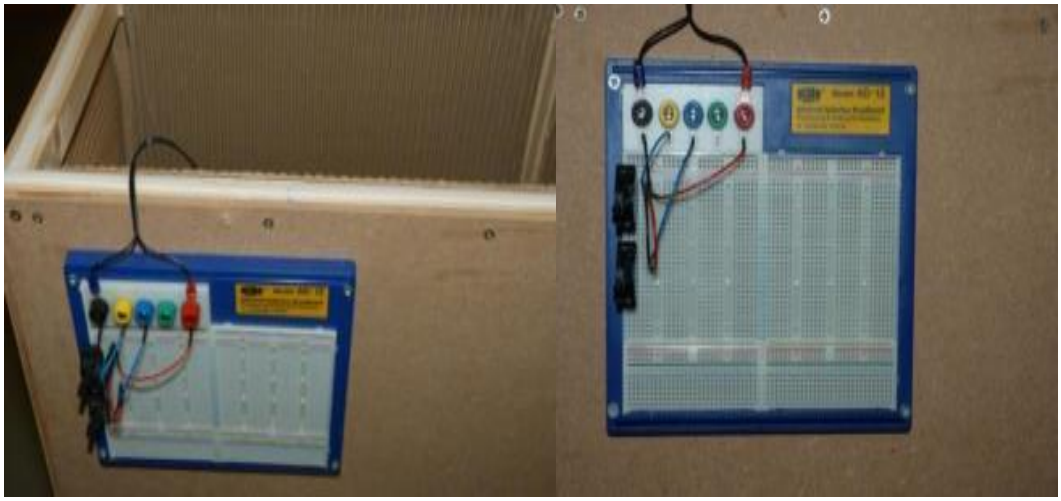

Figure 40 Air box Sample points for air pressure measurements.

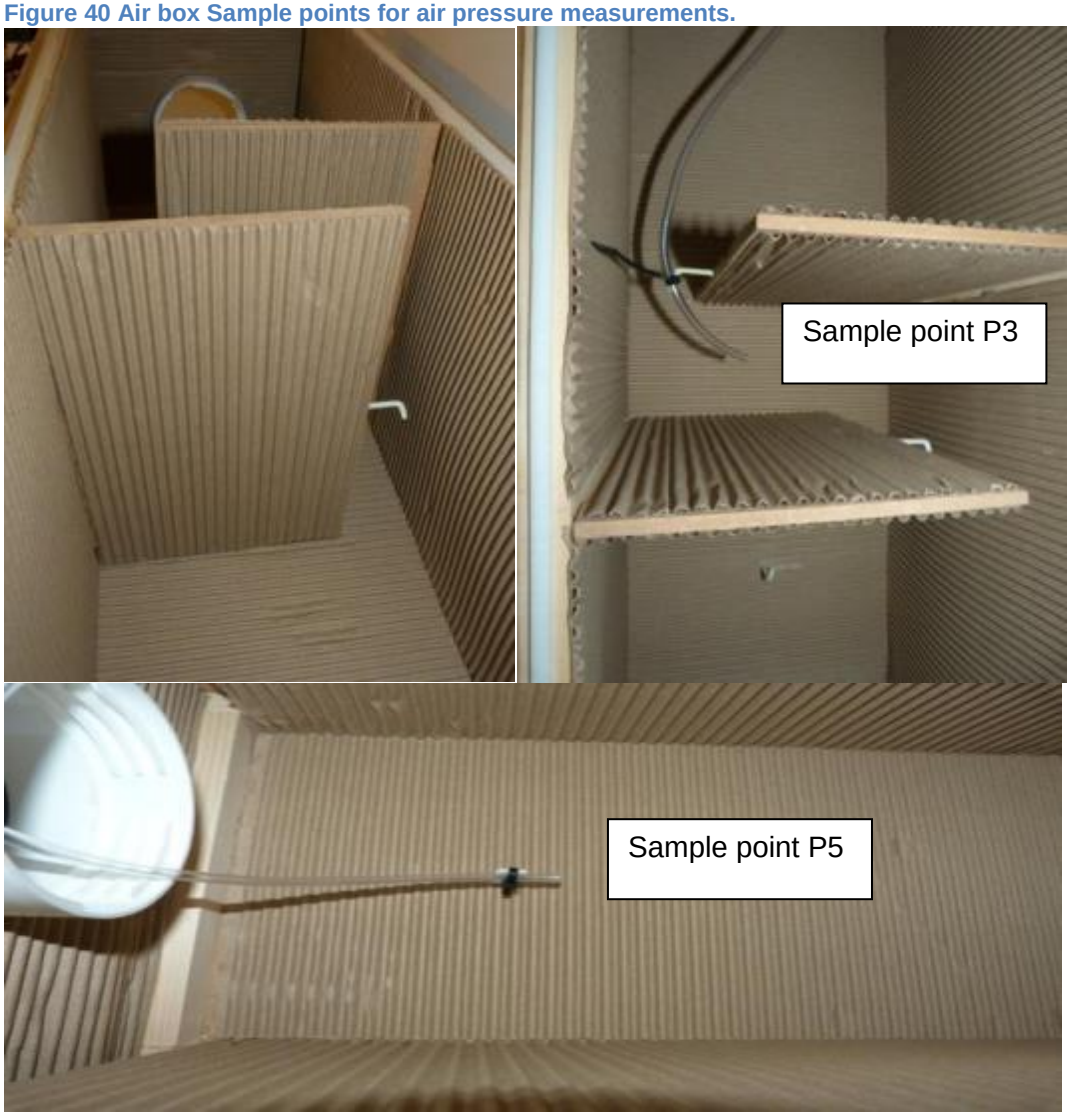

Figure 41 Millivolt measurements at pressure sample points.

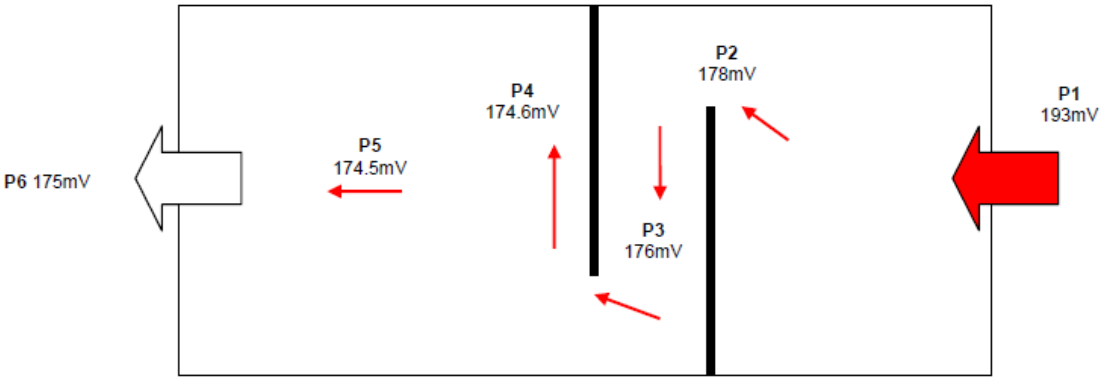

Table 5 Results of pressure sampling points.

Measuring point	Output Voltage (mV)	Pressure	
Reference CCGT Boiler inlet pressure	N/A	2.0 kPa	20 mbar
P1 Supply	193	1.26 kPa	12.6 mbar
P2 First baffle	178	1.11 kPa	11.1 mbar
P3 In-between baffles	176	1.08 kPa	10.8 mbar
P4 Second baffle	174.6	1.069 kPa	10.7 mbar
P5 Before exit	174.5	1.068 kPa	10.7 mbar
P6 Exit point	175	1.074 kPa	10.7 mbar

Where Pressure $(kPa) = Vs - \frac{Vout}{0.018P+0.04}$ Equation 14

So Vout $= Vs * 0.018 * P + Vs\ 0.14$ Equation 15

And Vout $- Vs * 0.014 = Vs\ 0.018 * P$ Equation 16

Therefore $P = Vout - Vs * 0.014 / Vs * \ 0.018$ Equation 17

Source; Instrument data sheet. (Freescale Semiconductor, 2012)

Observed pressure rise caused by the fan in the air box was minimal, maximum pressure rise at point of supply was 12.6 mbar.

Average pressure measured in the CCGT boiler is ~20 mbar at 410 MWe.

13 Difficulties with measuring potassium chloride as a vapor in the air box facility

The air box was constructed to evaluate if the monitoring of a radioactive isotope in the gas flow in a combined-cycle gas turbine power station could be simulated. To limit the radio-toxicity of the isotope in the air box potassium chloride (KCl), commonly known as low salt, was investigated as a starting point. KCl has a radioactive component ^{40}K that may be able to be measured without the constraints associated with producing the very short half-life isotopes that would be used when scaled up.

Previously experiments for detecting ^{40}K used a thallium-doped, sodium iodide scintillation counter in close proximity to the sample and substantial measuring periods (al, 2013) (~24 hr). Therefore, the use of low specific activity sources such as ^{40}K is limited by the ability to detect the radiation emitted by them efficiently.

At temperatures suitable for the air box to operate, the only option is to inject ^{40}K is as a solution with the hypothesis being that by allowing the residue to collect on the insides of the air box and on the detector this may provide sufficient material to obtain a sample count.

Ideally it would be preferred to monitor the ^{40}K as an aerosol; however, the melting point of ^{40}K at 770°C is well above the ability of the air box to handle the experiment. There are a number of possible methods that we could explore to establish the transit of potassium to a suitable detector which are discussed below:

1. Heating the KCl sample in a furnace tube assembly

The construction of a furnace tube assembly using a quartz glass tube, ceramic insulation and heating by a hot wire would achieve temperatures of 1200°C. This

temperature would produce a potassium vapor that can be directed in an airflow stream to a suitable detector.

The KCl sample could be introduced into the furnace when the furnace achieved a temperature ~1200°C, partly vaporizing the KCl sample. The resulting vapor would be channeled to a suitable scintillation detector for measuring. There are commercially available ceramic fiber cylindrical heaters that can reach 1200°C such as the high temperature range from Watlow (Watlow Supply, 2018).

Since KCl melts at 770°C and boils at 1500°C the sample would not reach boiling temperature using the ceramic heaters. It is postulated that some transit of the potassium vapor would take place from the sample at the maximum operating temperature of 1200°C.

2. Measurement using Collinear Photofragmentation and Atomic Absorption Spectroscopy

Alternatively, previous work conducted at Tampere University of Technology in Finland used a single particle reactor detected KCl vapor using Collinear Photofragmentation and Atomic Absorption Spectroscopy (CPFAAS) in combusted biomass fuels (Toivonen, 2013). The CPFAAS technique uses two lasers, one operating in the infrared spectrum emitting continuous wave light and the other in the ultraviolet range emitting 1ns pulses.

Figure 42 Biomass sample inserted into a single particle reactor and heated, the UV laser measures the refraction caused by the potassium chloride gas given off by the biomass sample. (Toivonen, 2013)

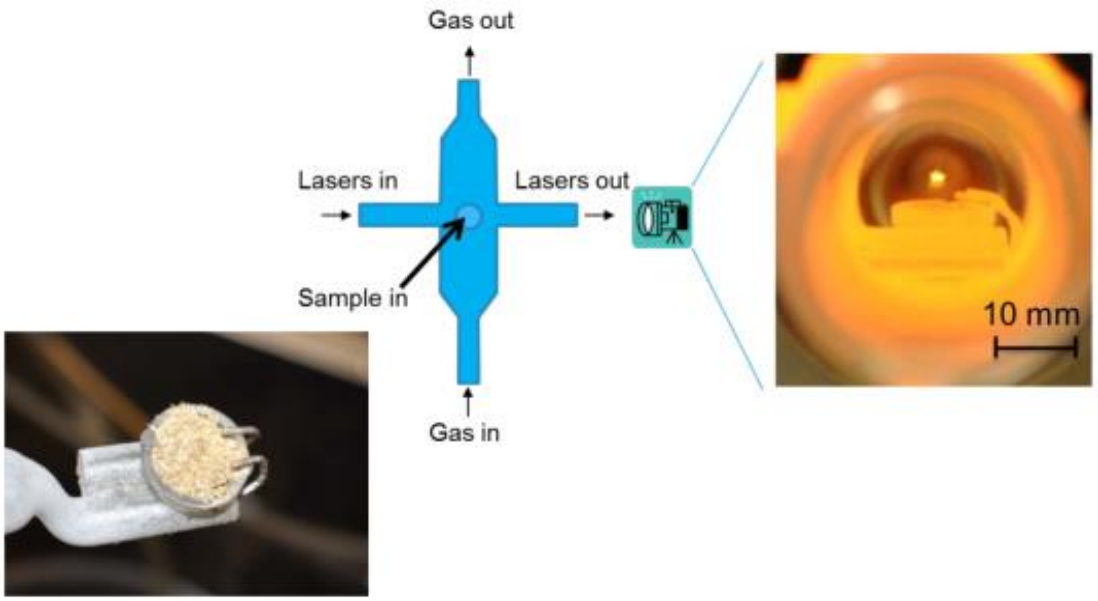

CPFAAS has been demonstrated in the detection of alkali chloride vapours (Toivonen, 2013). The technique utilizes a UV laser pulse to dissociate alkali chloride molecules to alkali and chlorine atoms. The resulting alkali atom concentration is monitored by a narrow bandwidth laser diode. The two beams are collinear aligned through the sample volume; this enables the detection of the temporally increased alkali atom concentration within the volume determined by the UV beam. The large absorption cross-sections and the narrow absorption profiles of the alkali atoms favour their detection.

Figure 43 CPFAAS technique to disassociate alkali chloride molecules (Toivonen, 2013)

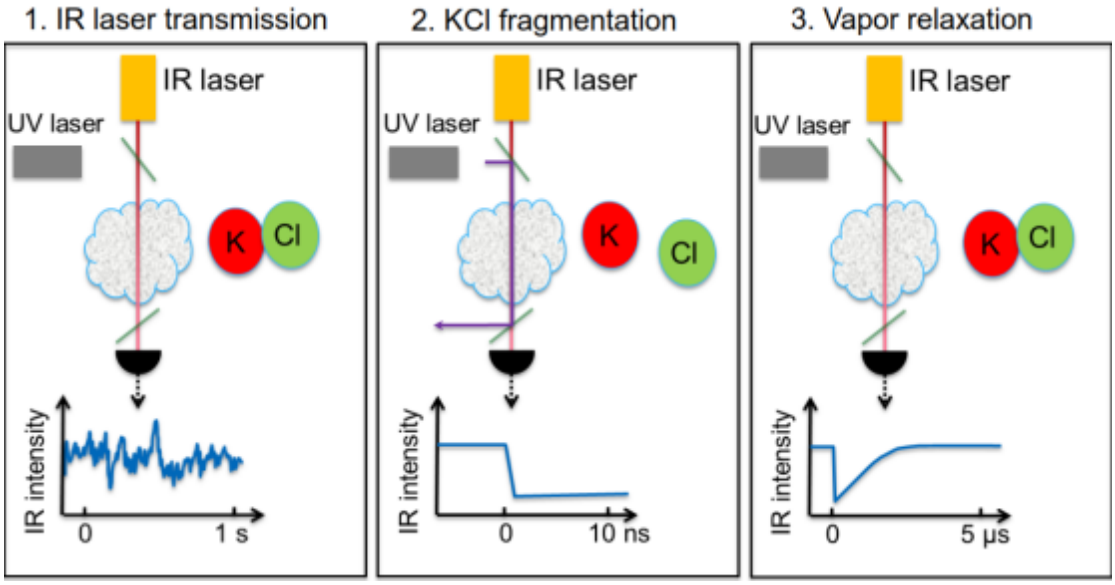

The measurement of potassium chloride using the CPFAAS technique requires specialist equipment. The simplest, most cost effective method to obtain proof of principle that we can detect radioactive potassium chloride vapour is by heating it to melting point is by using a ceramic heater.

14 Potassium chloride test rig design

Our primary design parameter for the test rig is to heat a sample of potassium chloride to melting point in the attempt to transfer the resultant vapour to a collection medium for measurement using a scintillation detector.

Previous experiments measuring ^{40}K with a scintillation detector require a shielded collimator, close proximity to the sample and substantial measuring periods (~24 hrs). The test rig's role is to provide a good degree of transit of the potassium chloride to obtain a sample for subsequent radioactive count sampling.

14.1 Construction of a ceramic furnace tube assembly

The potassium chloride sample (solution) was introduced into the ceramic furnace via a ceramic sample boat when the furnace achieved a temperature ~800°C, melting

the potassium chloride in solution. The resulting vapour was channelled to a steel plate to condense and the resultant condensate collected in laboratory glassware for subsequent scintillation counting.

KCl melts at 771°C and boils at 1500°C therefore a pure KCl sample would not be fully vaporised using the ceramic heater. It is postulated that the potassium chloride vapour would transit as a vapour, condense and be collected for later counting.

Selection of equipment - Initial equipment set up

The test rig was constructed from a ceramic heater, a 550°C heat gun and steel condensing plate to cool the vapour and direct into a collection glassware beaker. The heat gun to provided motive force to encourage the sample once vaporised to transit as a vapour through the rig to the container.

Figure 44 Ceramic heater used to heat potassium chloride to melt temperature.

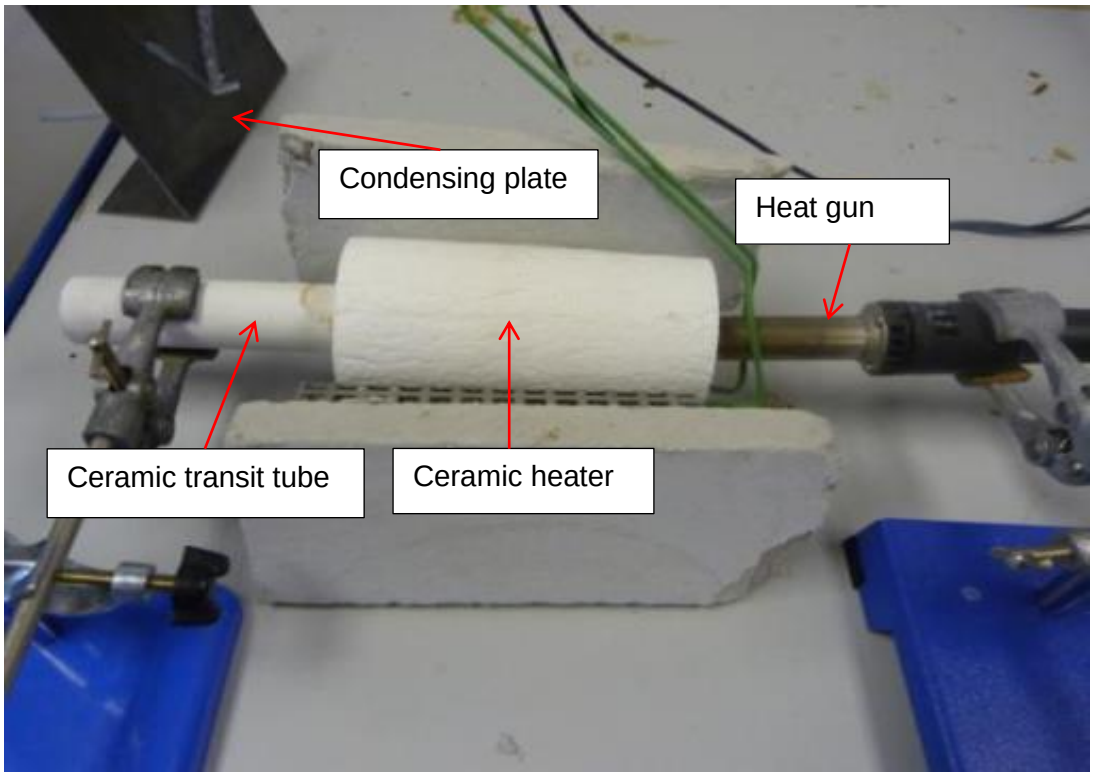

The solution was placed in the ceramic boat and heated to 800°C and the vapour was directed along a ceramic tube to the condensing plate. Using water as a sample,

the transit of the vapour was observed along the tube to the condensing plate and into the collection beaker. When a potassium chloride solution was substituted for the water only small quantities of vapour escaped and none could be collected in the sample jar using this method.

Figure 45 Potassium chloride solution introduced into the heater using a ceramic boat.

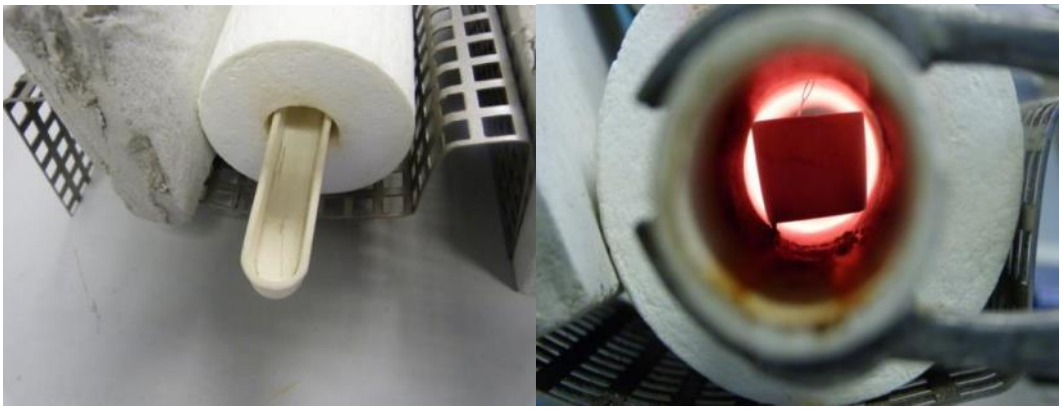

Using a fully saturated KCL solution (35 g/100mL at 20°C), the heat sink failed to condense sufficient quantities of vapour to obtain a sample. KCl reached its melting point (770°C) and was deposited on the internal surfaces of the ceramic heater, however the ceramic boat containing KCL solution failed possibly due to the thermal shock associated with the KCL solution being applied.

Figure 46 Steel plate used to condense the vapour and allow collection into a glass beaker.

Figure 47 Condensing plate failed to capture sufficient vapour; majority was lost to the air.

Figure 48 Ceramic boat failed in the heater probably due to the thermal shock associated with introducing the potassium chloride solution.

14.2 Test Rig modification

An alternative heat sink arrangement using a glassware condenser with a water cooling system was added to aid with condensing the vapour produced by the heater. Three potassium chloride water solutions were made up of 10%, 20% and 50% strength. Each was introduced internally to the heated tube via a squeeze bottle, the resulting vapour was directed along the tube into the condensing glassware and sample jar, the test was stopped when a 20 ml sample was obtained.

Figure 49 Modified collection system using a stainless steel tube and condensing glassware

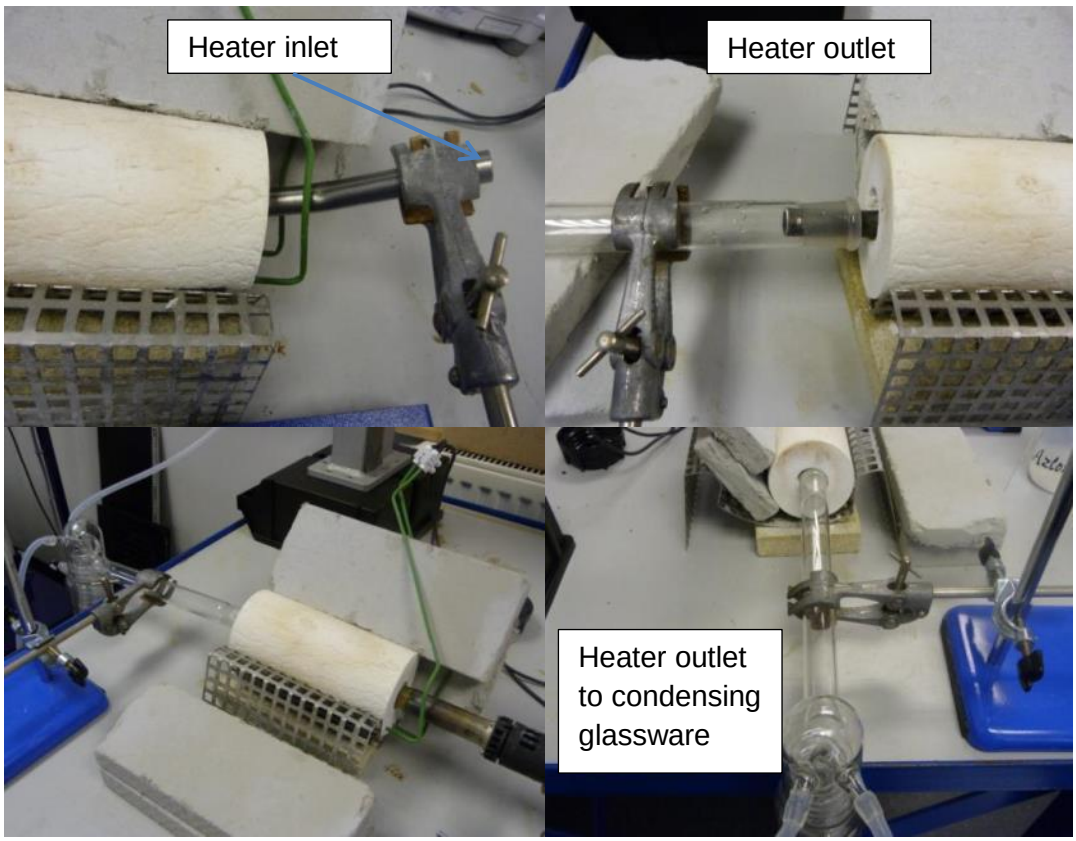

Figure 50 Introducing the potassium solution into the stainless steel tube.

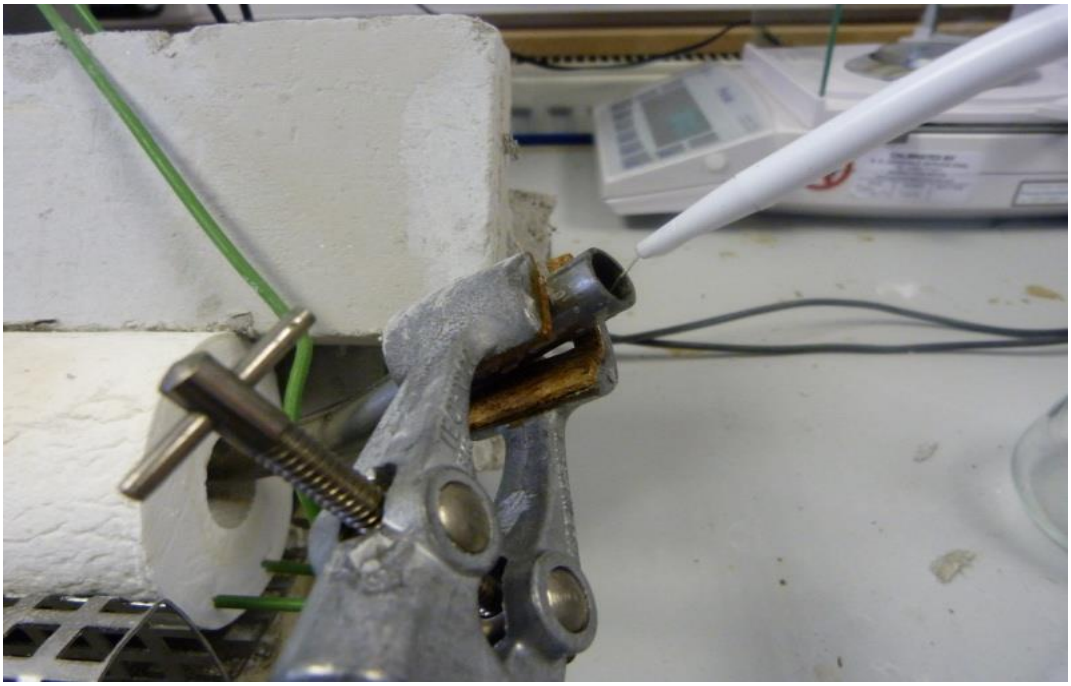

Figure 51 Visible potassium chloride deposits carried through the stainless steel evaporator tube.

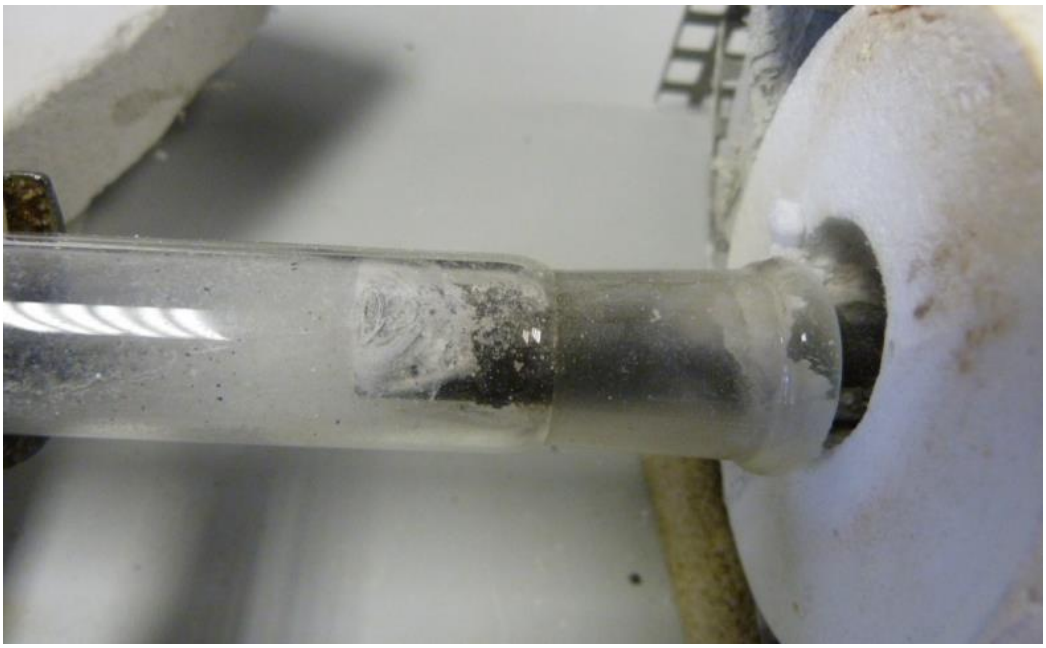

Vapour was observed from the exit end of the stainless steel tube during the test which collected on the tube and glassware indicating that water vapour containing

potassium had been transported as a vapour. When the tube was cooled and removed from the ceramic heater, deposits of potassium could be observed along the external tube length.

With the 50% solution the tube quickly became blocked by the build-up of crystalline KCl restricting flow through the tube.

Figure 52 heavy potassium chloride deposits where the vapour escaped from the outlet end of the stainless steel tube.

14.3 Test Samples

The three test rig samples where then counted using a NaTl(I) counter in a lead collimator over a long count period (24 hr) to cater for the relatively low specific activity of ^{40}K.

Figure 53 Test samples at 10%, 20%, 30% and 50% solutions.

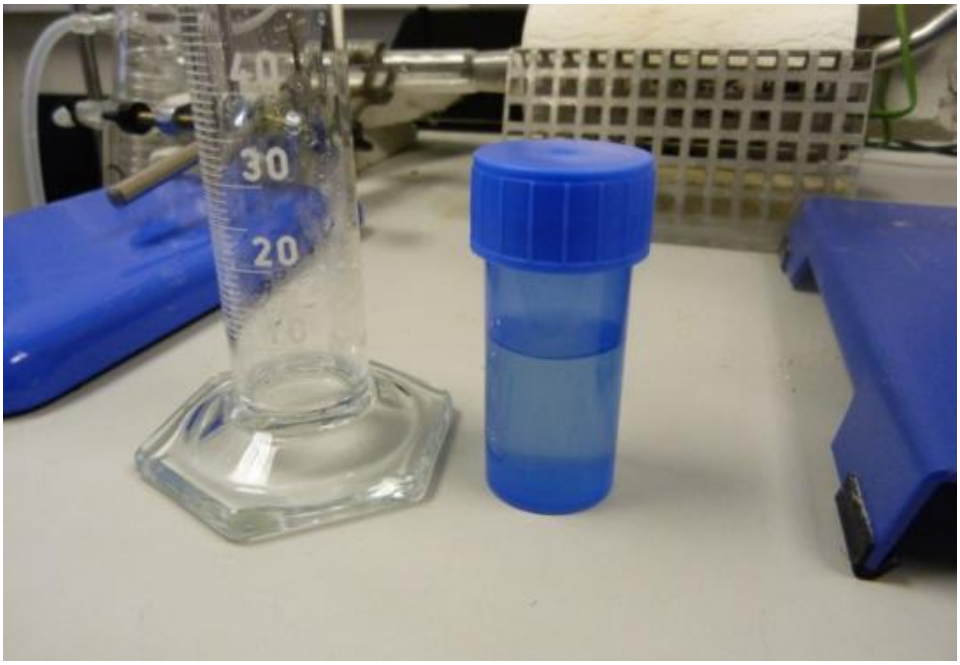

Figure 54 Lead blocks where used to shield the samples during counting.

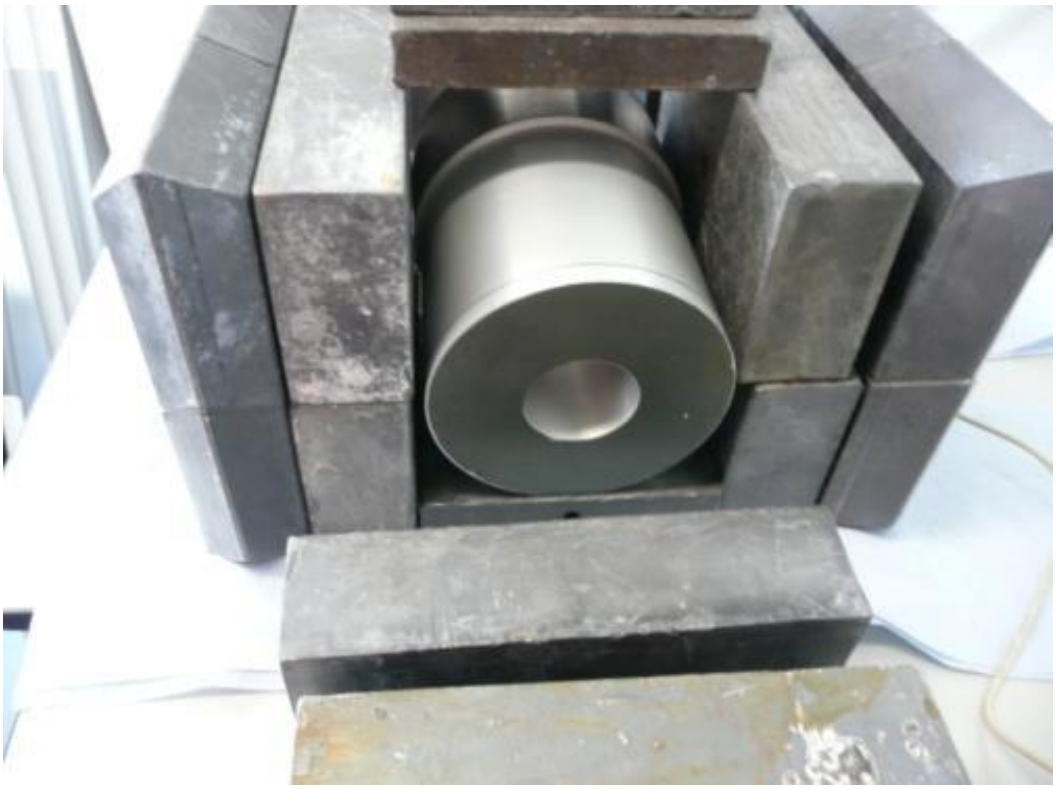

Figure 55 Potassium chloride sample count over 24 hours of 10, 20%, 30% and 50% samples.

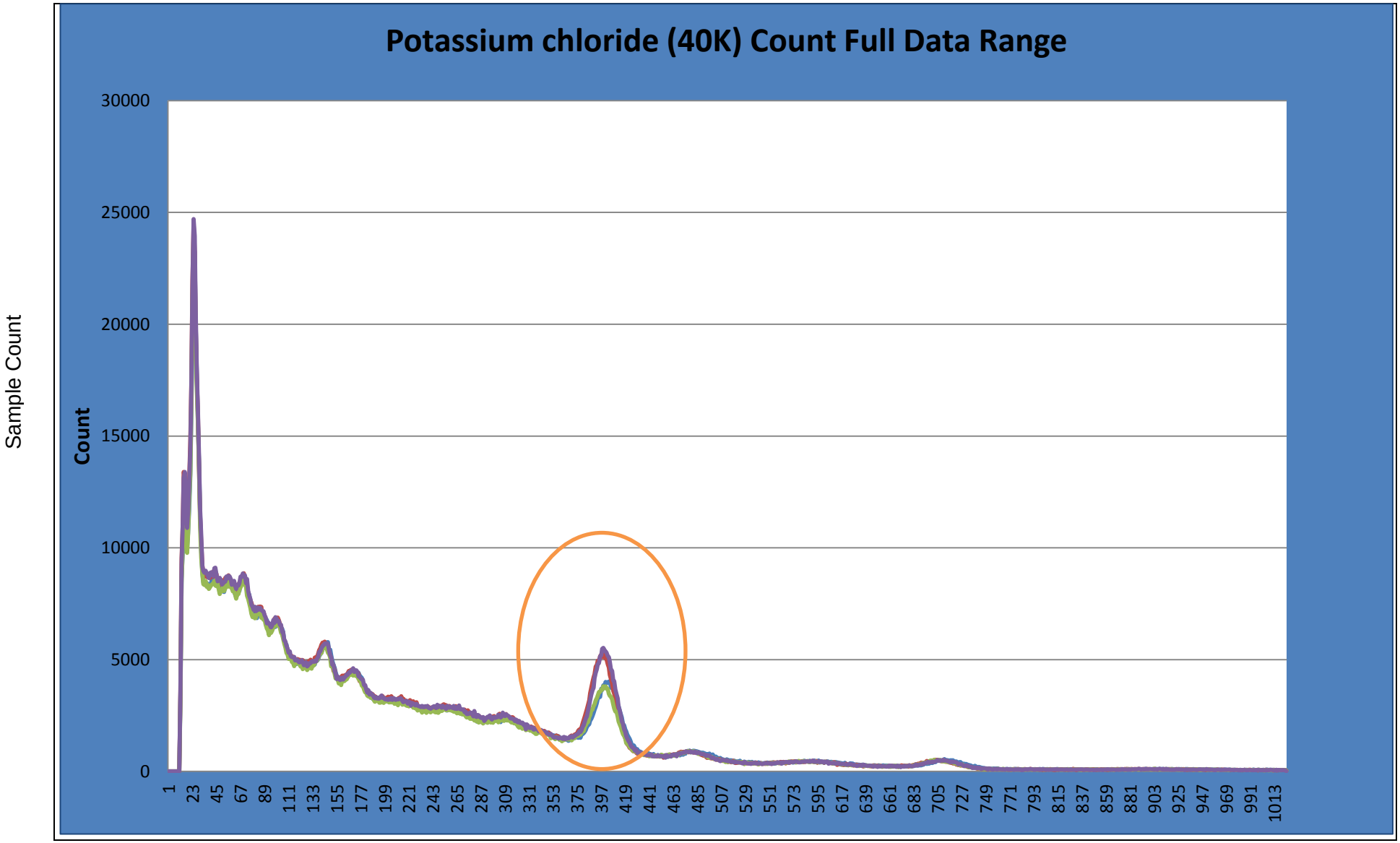

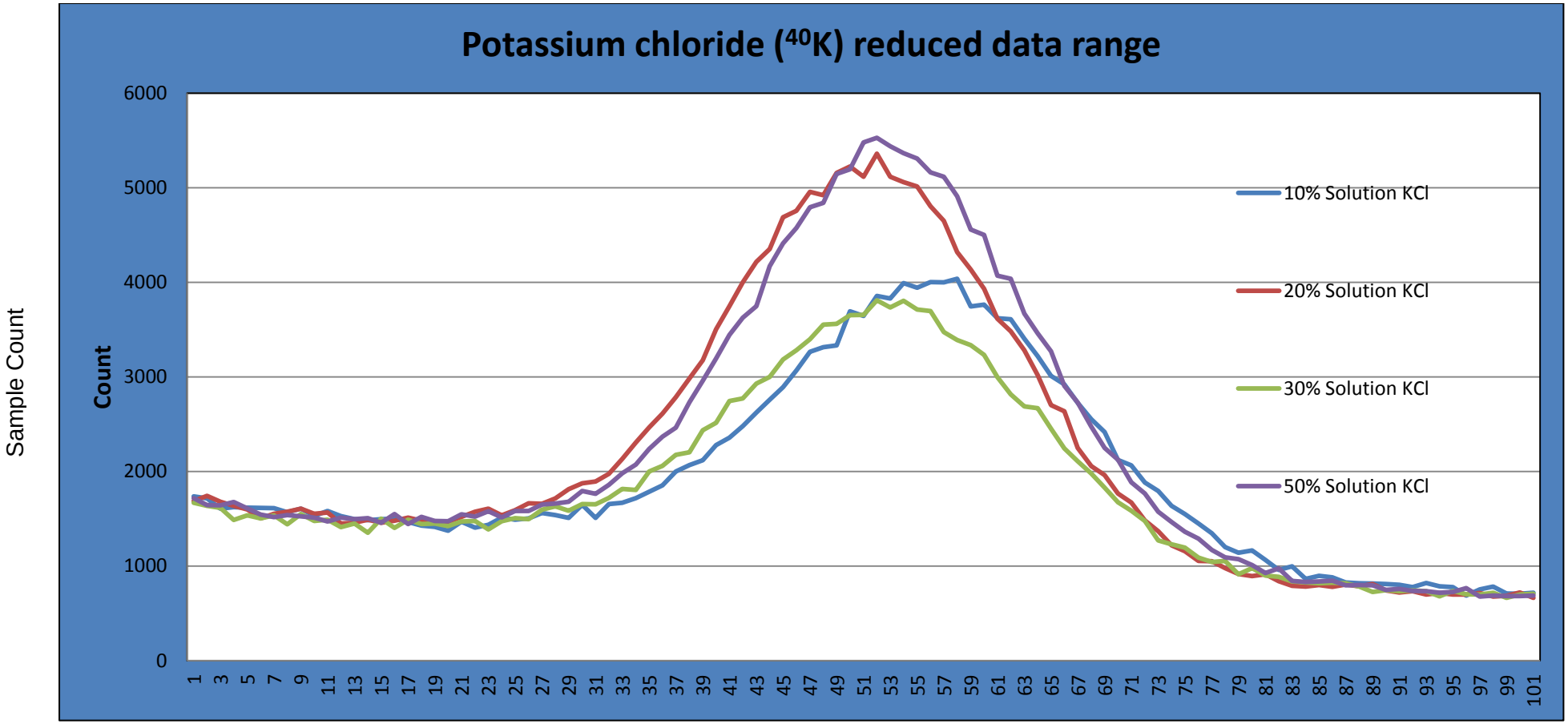
Potassium chloride (^{40}K) reduced data range
Count
Sample Count
Channels
10% Solution KCl
20% Solution KCl
30% Solution KCl
50% Solution KCl
0
1000
2000
3000
4000
5000
6000
1 3 5 7 9 11 13 15 17 19 21 23 25 27 29 31 33 35 37 39 41 43 45 47 49 51 53 55 57 59 61 63 65 67 69 71 73 75 77 79 81 83 85 87 89 91 93 95 97 99 101

14.4 Carryover of potassium chloride solution into sample

Figure 57 indicates that ^{40}K is present in all samples. ^{40}K emits a gamma ray with energy of 1461 keV (Universities, 2009). Higher activity levels would be associated with the higher solution concentrations of ^{40}K (if the transport mechanism is assumed to be independent of the concentration of KCl), this proved not to be the case. This indicated that some solution had not been fully evaporated in the steel tube and carry-over (non-vaporised solution) had taken place into the condenser and sample jar.

In order to disprove the carry-over theory, a hot plate was used to boil a solution of potassium chloride using the same condenser and sample jar. By boiling the solution at atmospheric pressure and collecting the condensed vapour it was expected that the vapour would not contain any ^{40}K. The samples were counted using the same scintillation counter equipment and the spectrum results verified that no potassium chloride was carried over in the sample.

Figure 56 A solution of potassium chloride was boiled and the vapour condensed into a sample jar.

14.5 Improving the residence time in the furnace and adding superheat to the sample.

To overcome the carry-over of non-vaporised solution into the collection glassware, a modified heat exchanger was manufactured using 5 mm diameter stainless steel tube which was formed into a double flow coil; the coil was located within the ceramic heater.

The intention was to allow the injection sample solution a longer residence time in the heater. The coil has a double flow to allow a return through the heater once vaporised. This would ensure that no non-vaporised solution would be carried forward into the collection glassware.

Figure 57 Modified heat exchanger using a double flow stainless steel coil to increase the residence time of the potassium chloride solution in the furnace.

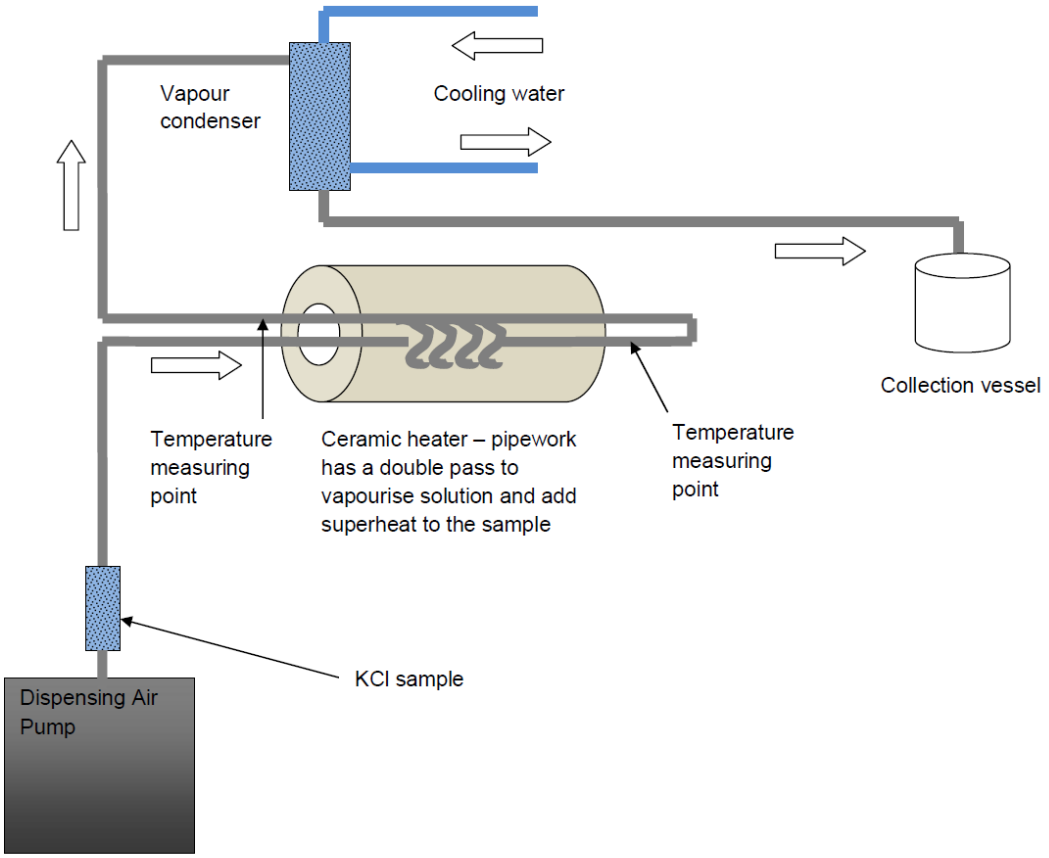

14.6 Improving the sample flow through the heater

The rate of injecting the solution into the tube had to be controlled, as too much solution would increase the likelihood of non-vaporised solution carried over into the sample. Manually controlling this proved problematic and hence a more consistent method of feeding the solution into the heater was required.

To alleviate the sporadic feed rate of the solution into the heated tube, a syringe containing a 10-ml sample was electronically dispensed into the tube inlet, using an electronically-controlled motorized feed pump.

To determine the feed rate at which no carryover occurred, a solution of distilled water mixed with a red food dye was tested at differing feed rates until no carry over was observed on a sample paper located at the vapour outlet side of the heater.

Figure 58 Electronic feed system for controlling the sample flow through the heater coil.

The feed rate was adjusted until no carryover was observed on the test paper fitted at the vapour outlet of the equipment.

Table 6 Feed rate into heater coil to determine carry over conditions.

Red dye test to determine feed rate for carry over		
Heater temperature	850℃	
Heater current	1.7A	
Red dye solution temperature	18°C	**Result**
Feed rate	2ml/min	Fail
	0.9ml/min	Fail
	0.6ml/min	Pass
	0.4ml/min	Pass

14.7 Feed rates

The red food dye solution was carried through the heater coil when the feed selection was set at 2 ml/min and 0.9 ml/min. When the feed rate was reduced to 6 ml/min no non-vaporised food dye was visible on the sample paper. A second test was conducted using a feed rate of 0.4 ml/min with a clear result.

Figure 59 Feed rate result sheets, 2ml/min and 0.9ml/min showing carry over of non-vaporised food dye.

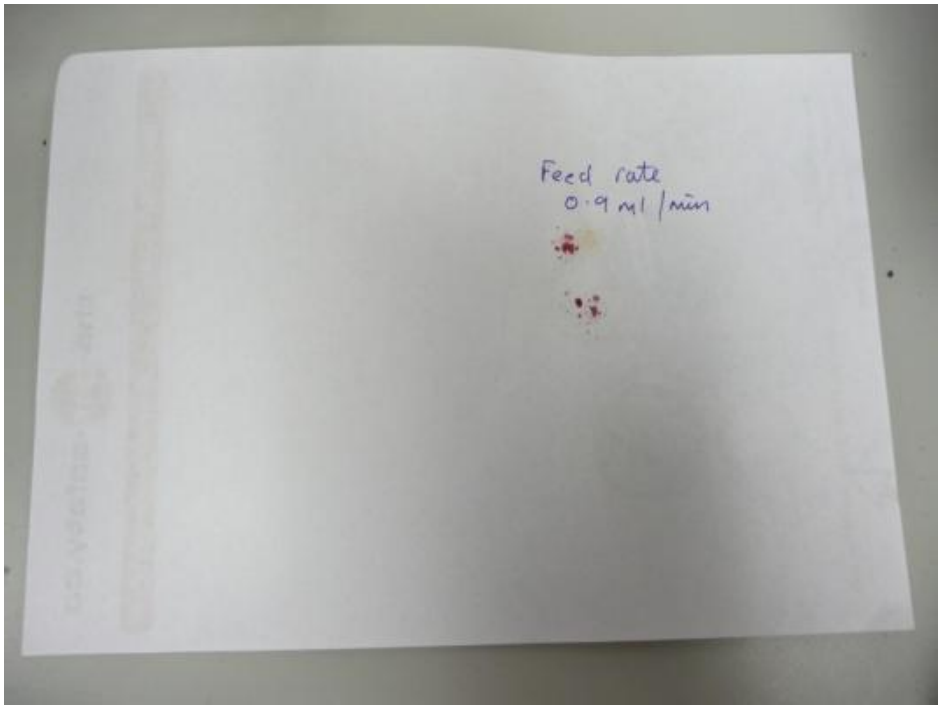

Once a clear sample was obtained at a feed rate of 0.6 ml/min, the experiment was run again using a potassium chloride solution of 10%, 20% and 30%. To ensure no carryover occurred, the feed rate was set to 0.4 ml/min.

Table 7 Potassium chloride injection at low feed rate into heater coil.

23.03.15			Test Results	
Lancaster Chemical Laboratory	Heater Temperature	Feed Temperature	Feed rate	Results
Test 1 10% Solution	850°C	18°C	0.4ml/min	15ml sample obtained
Test 2 20% Solution	850°C	18°C	0.4ml/min	10ml sample obtained before tube became blocked with KCl
Test 3 30% Solution	850°C	18°C	0.4ml/min	1ml sample obtained before tube became blocked with KCl

Figure 60 Potassium chloride solution injected into the stainless steel heater coil.

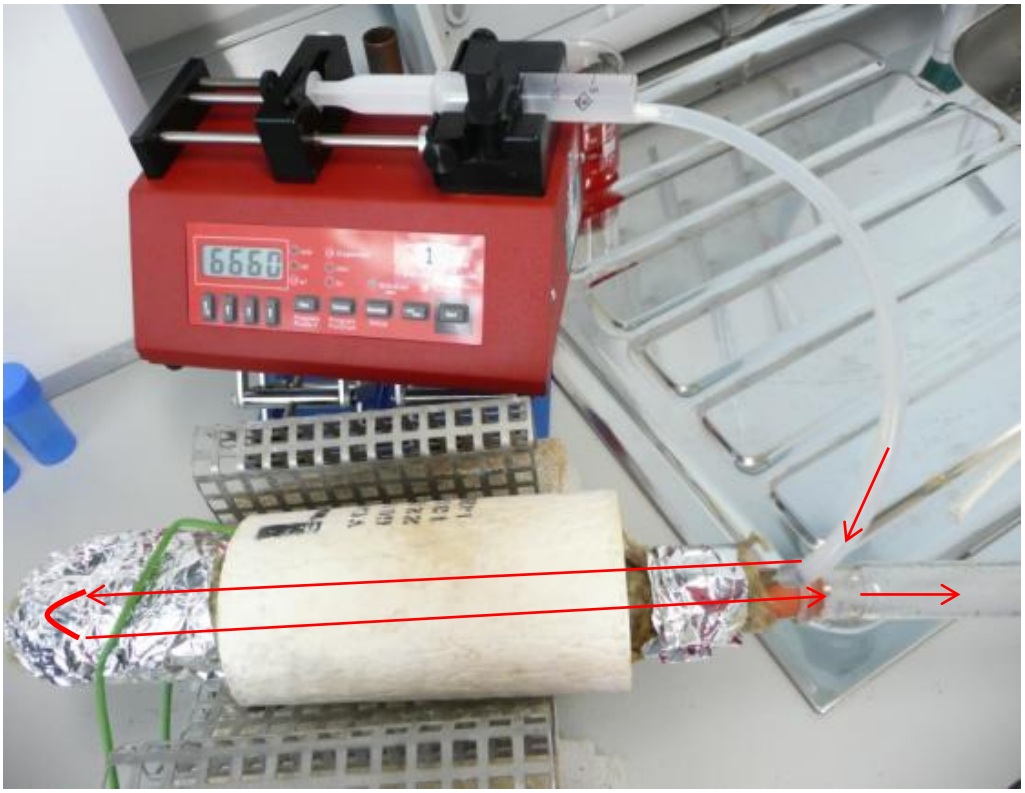

Figure 61 Vapour from the heater outlet condensing in glassware prior to collection.

Figure 62 Results from 10% potassium chloride solution.

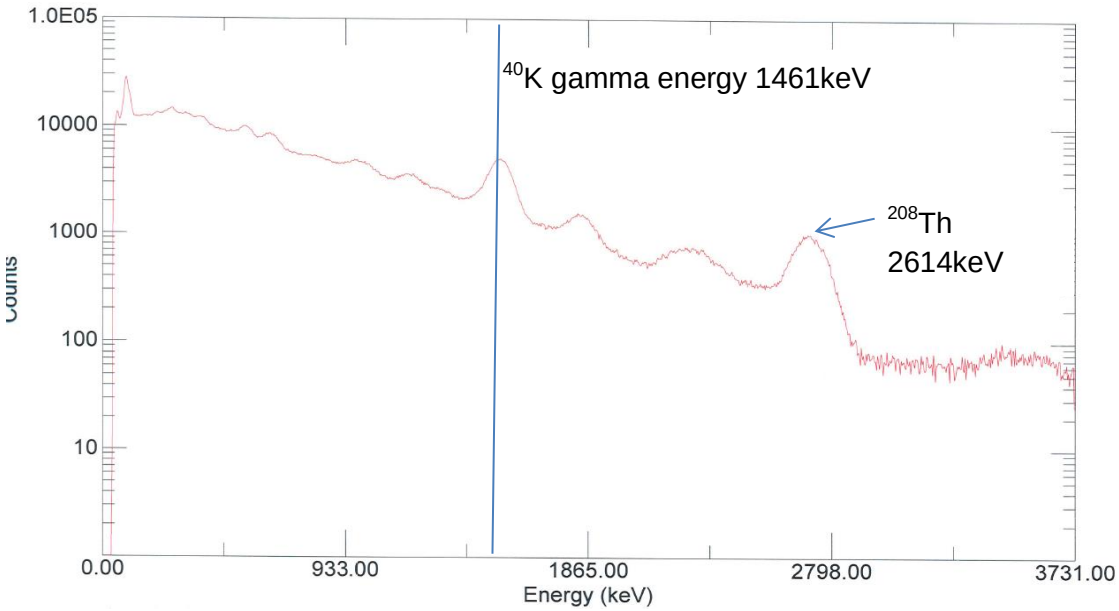

Figure 63 Results from 20% potassium chloride solution.

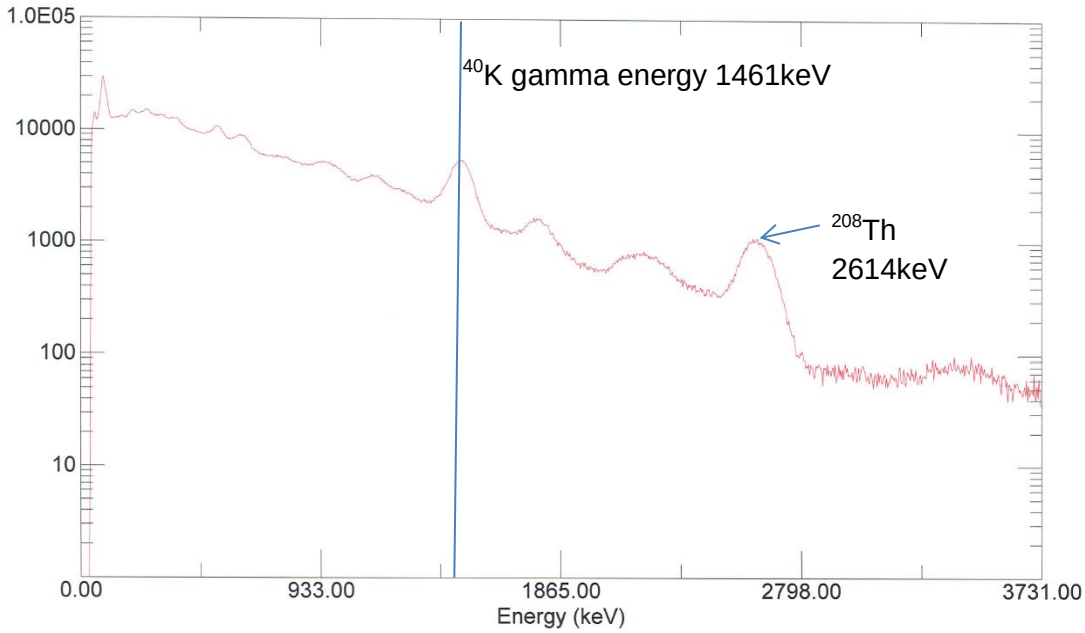

Figure 64 Results from 30% potassium chloride solution.

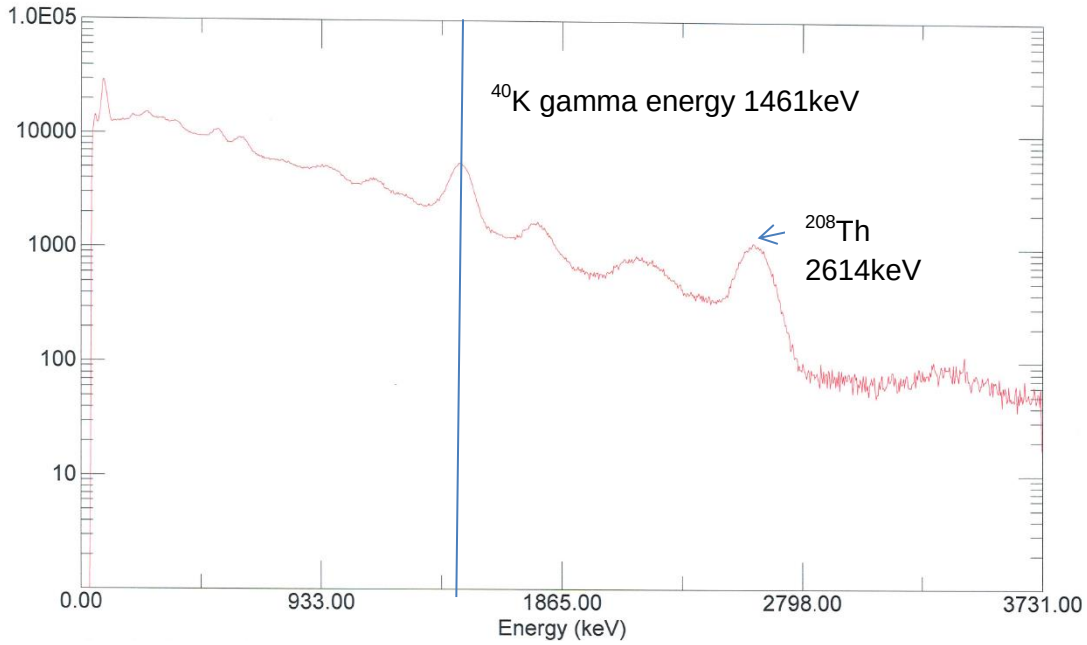

15 Results of potassium chloride sample scintillation measurements

The tube heater was used to allow a sample of potassium chloride to be collected and measured. The measurement period was 24 hours therefore it would not be feasible to use the air-box method. The collection of a vaporised sample of potassium chloride in solution was thought to be the easiest method to prove the hypothesis that radioactive vapour could be detected using a scintillation detector.

Ensuring that the feed rate of ^{40}K solution into the tube heater remained constant to avoid carryover was fundamental in obtaining consistent results. The electronic feed rate instrument was set at 0.4 ml/min as this provided sufficient heater residence time to ensure that all the solution was vaporised in the heater tubes and no water carryover occurred into the condensing glassware.

Increasing the percentage of potassium chloride in solution reduced the sample volume obtained by the experiment. With higher concentrations of potassium chloride solutions, the heater tube quickly became blocked with potassium chloride which

reduced the sample volumes. Sample volumes were collected from 10%, 20% and 30% potassium chloride solution concentrations.

The 3 samples were counted using a NaTl(I) scintillation detector contained within a lead collimator for a period of 24 hours. The results are shown in Figure 62 Results from 10% potassium chloride solution, Figure 63 Results from 20% potassium chloride solution and Figure 64 Results from 30% potassium chloride solution.

The results show that gamma rays with an energy at 1461 keV were detected which is a gamma energy signature associated with ^{40}K and ^{208}Thalium 2614keV (Universities, 2009).

16 Conclusion

The hypothesis; Detection and measurement of a radioactive tracer contained in a water ammonia solution when heated and vaporised in to a gaseous phase.

The results in this thesis demonstrate that radioactivity can be detected when a radioactive substance in solution is vaporised in a tube heater, the vapour is condensed and the water sample measured using a scintillation detector.

The experiment used potassium-40 as the radioactive element due to its low toxicity hazard, availability and water solubility.

The solution was heated beyond its critical temperature[7] in the tube heater. As the solution was heated, the pressure and temperature increased in the tube heater and as the critical point of the solution (374°C) was passed. The KCl and H_2O molecules converged resulting in a homogenous supercritical fluid, the higher temperature weakening the intermolecular forces allowing transfer of potassium-40 to the sample jar.

[7] Critical temperature for water is 374°C/647K. Above this temperature water cannot exist as a liquid irrespective of pressure.

However, ^{40}K would be unsuitable to inject into a high-temperature, industrial, steam-generating boiler due to the metallurgic limitations of chlorides causing pitting corrosion of steels used in boiler tubing at high temperatures. The phenomenology of water-containing chlorides causing pitting corrosion is essentially the formation of a micro-environment of hydrochloric acid established within the surface pits; this lowers the pH and increases the chloride ion concentration, resulting in electrochemical attack (Ma, 2012).

Common radioactive isotopes used in industrial closed system leak detection would not be suitable for injection into the water side of a power plant heat recovery steam generator because any leakage into the gas side of the generator would be exhausted to the boiler stack and released to the local environment. The relatively long half-lives (measured in hours) and high gamma energies of these radioisotopes would present a radioactive hazard to people and the environment in the exhaust plume drop out zone from the stack. Many of the radioisotopes are also chloride-based and thus pose boiler corrosion problems (see Table 3).

Medical radionuclides used in photon emission tomography (see Table 4) provide high gamma energies which facilitate detection and short half-lives to limit radioactive hazard. Nitrogen-13 is produced in the form of $^{13}NH_3$ has the potential for use in power station boiler feedwater systems due to its compatibility for injection for into the boiler water stream, its gamma radiation energy of 511 keV and because it has a short half-life (~10 minutes).

One of the selection criteria of a suitable radiotracer is that the radiotracer's physio-chemical nature should be compatible with the fluid being traced. Boiler feedwater is dosed with ammonia (NH_3 aqueous solution) to increase the pH and limit the effects of corrosion on the internal boiler steel components. Ammonia solution is injected into the feedwater by a positive displacement pump connected to a standard 1000

litre intermediate bulk container (IBC) containing ammonia at 20% solution. The injection of $^{13}NH_3$ at this injection point would provide a suitable method to introduce the radiotracer.

16.1 Radiotracer detection

Radiotracers emitting gamma rays can be detected by suitable scintillation detectors located in the gas exhaust stack sampling points near the stack exit points. The boiler is designed to have a very high Reynolds number, ensuring the exhaust gas is homogeneous in its heat delivery to the boiler tubes, and to ensure that the gas turbine exhaust emissions are monitored accurately for statutory emissions requirements.

Typical detectors suitable for 511 keV gamma rays produced by $^{13}NH_3$ are thallium-doped sodium iodide NaI(Tl) coupled to photomultiplier tubes (PMTs). With the relatively recent discovery of bismuth germinate $Bi_4GE_3O_{12}$ (BGO) and lutetium orthosilicate Lu_2SiO_5 (CE) (LSO), most detectors based on these materials are also suitable because of higher detection efficiencies for gamma-ray detection.

The next logical stage would be the construction of test rig to inject ^{13}N into a boiler system with simulated gas turbine exhaust conditions. The boiler would be designed to allow a simulated leak to develop; the exhaust gas would then be passed through a tube containing a scintillation detector to evaluate if the ^{13}N has been transported as a vapour, validating the results of the potassium chloride experiments.

17 Future Work

The continuing economic challenges of the traditional thermal power generating portfolio of coal and gas power plants are heightened by the increasing installed

generating capacity from renewable sources. Renewable sources of power generation are scheduled by National Grid as must run[8] generation.

The construction of new nuclear power plants requires large capital investment, often beyond the potential for a single company to fund without a consortium effort. The governmental and public concerns to generate electrical power by nuclear methods means that in many countries, new nuclear is not an option for new build power production.

This makes the availability of existing and future fast response CCGT power plants increasingly important. Unavailability caused by boiler failure results in considerable downtime, the importance of preventative maintenance based on inspection and testing has never been higher. The opportunity to enhance the boiler leak detection capability by radiotracer injection should be the subject of further research.

17.1 Test rig construction

The construction of a test rig to conduct full scale temperature testing of a medical radionuclide such as ^{13}N is the next logical step in testing the hypothesis. The structure should be able to withstand exhaust gas exit temperatures in the region of 600°C that can be generated by a small model gas turbine engine. The test rig should be connected to a fume hood or external discharge point with minimal back pressure to ensure the test rig does not become pressurized.

A heat exchanging mechanism (water radiators) should be installed to remove heat from the system and to provide an injection point for the aqueous ^{13}N solution. The heat exchanging mechanism should also promote homogenous mixing of the gas turbine exhaust gas flow and the injected radionuclide.

[8] Must run generation is scheduled by the National Grid to generate before any other sources of generation. Nuclear generating plant and renewables are classed as must run plant.

A lead shield should be utilized to prevent a direct shine path from leak point to detector. The shield should be arranged to allow free gas flow around the baffles and prevent a direct radiation shine path. The half value layer of lead (Pb) for 511keV Photons is 4 mm. A thickness of 39 mm of lead will provide a 1000 times attenuation factor. (Drugs.com, 2017). Due to temperature constraints it may be advisable to substitute lead for steel plates or tungsten.

The exhaust route for the boiler would need to be directed through a suitable filtration system and high level discharge to ensure that a radiation hazard would not exist at the exhaust discharge point. Activated charcoal is a form of carbon processed to have small, low-volume pores that increase the surface area available for adsorption of the vaporized solution. Activated carbon combined with a silica gel absorber would help to reduce any radioactive hazard from the exhaust discharge route.

The short half-life (10 minutes) requires that the cyclotron production facility for ^{13}N should be in close proximity to the test rig. The useful lifetime for ^{13}N is limited; the fraction remaining after 30 mins is 0.124. The limited lifetime of ^{13}N requires a production facility and a test facility to be close by. The proximity of Addenbrookes hospital, Hills Road, Cambridge, UK is close to the Cambridge University facility; this may provide synergies between a production facility and a test laboratory.

Figure 65 Boiler test rig suitable for injecting a radioactive tracer such as ^{13}N

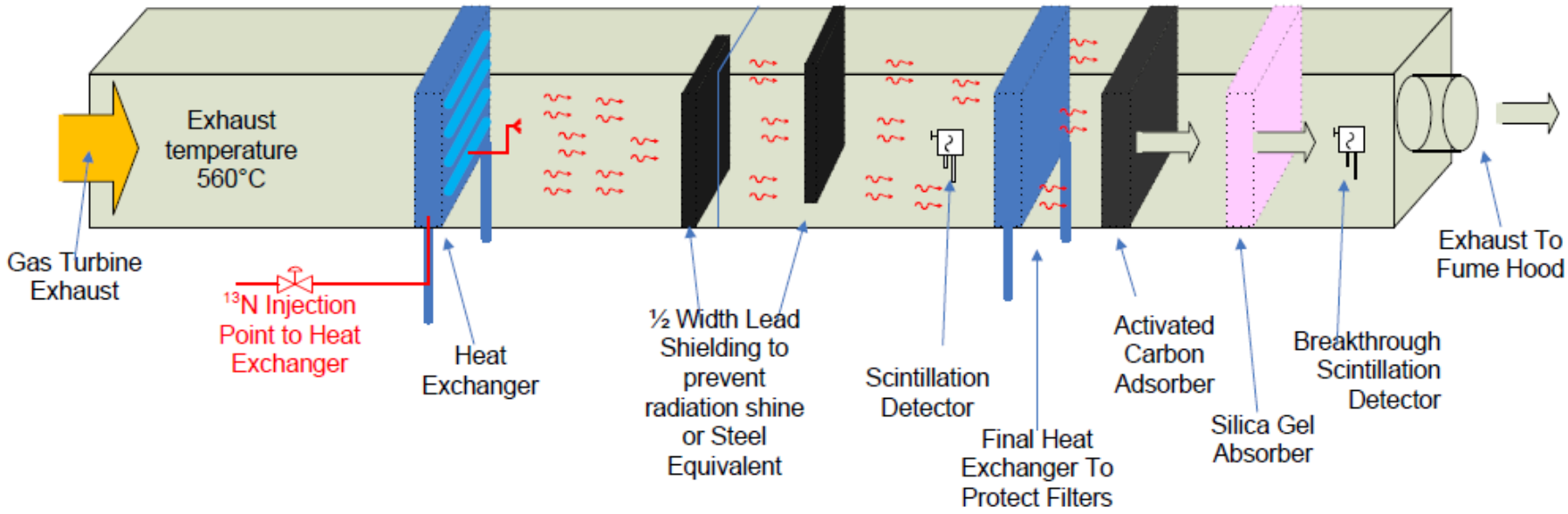

Bibliography

Freescale Semiconductor, 2012. *MPX 5700 Series - Integrated silicon pressure sensor.* [Online]
Available at: https://www.nxp.com/docs/en/data-sheet/MPX5700.pdf
[Accessed 03 2018].

al, A. P. e., 2013. *A Thalium doped sodium iodide well counter for radioactive tracer applications with naturally abundant K40, (2013.* Lancaster, Uk : Engineering Department Lancaster University .

Albina, 2005. *Theory and experience on corrosion of waterwall and superheater tubes of waste to energy facilities..* [Online]
Available at: http://www.seas.columbia.edu/earth/wtert/sofos/Albina_thesis.pdf
[Accessed March 2018].

Bart et al, 2004. Preventing Boiler Corrosion,. *Waste Management World,* Issue Setember.

BEIS, 2., 2016. *Statistics at BEIS,* London: Busness Energy Industrial Strategy .

Carson, B. & Coleman , K., 2009. *116379556-EPRI-Field-Guide-for-Boiler-Tube-Failures.* Palo Alto, Calafonia USA: Electric Power Research Institute.

Cushman-Roisin, B. 2., 2012. *Effective smokestack height.* [Online]
Available at:
https://thayer.dartmouth.edu/~d30345d/courses/engs43/smokestacks.pdf

Department for Business, E. a. I. S., 2016. *Dynamic Dispatch Model,* s.l.: s.n.

Drugs.com, 2017. *Ammonia N - 13.* [Online]
Available at: https://www.drugs.com/pro/ammonia-n-13.html
[Accessed 03 2018].

GE, 2018. *GE Power.* [Online]
Available at: https://www.gepower.com/gas/hrsg
[Accessed 3rd February 2018].

General Electric, 2., 2012. *Boiler deposits, occurance and control.* [Online]
Available at:
https://www.suezwatertechnologies.com/handbook/boiler_water_systems/ch_12_boilerdeposits.jsp
[Accessed 1 July 2018].

Grid, N., 2010. *The Grid Code.* [Online]
Available at:
https://www.nerc.com/comm/PC/Integration%20of%20Variable%20Generation%20Task%20Force%20IVGT/Sub%20Teams/Interconnection/UK_Grid_Code.pdf
[Accessed August 2018].

IAEA, 1995. *IAEA-TECDOC-899,* Vienna: IAEA.

IAEA, 2009. *Tech doc 468 radionuclides, 2. Cyclotron produced, Physical characteristics and production methods,* s.l.: IAEA.

IAEA, 2., 2009. *Leak Detection in Heat Exchangers and underground pipelines using radiotracers,* s.l.: IAEA.

Institute, G. C., 2018. *Global CCS Institute.* [Online]
Available at: https://hub.globalccsinstitute.com/publications/annex-iii/2-gas-fired-combined-cycle-power-plants
[Accessed 3rd February 2018].

International, P. E., 2012. *Achieving high efficiency and flexibility in the field.* [Online]
Available at: http://www.powerengineeringint.com/articles/print/volume-20/issue-5/features/achieving-high-efficiency-and-flexibility-in-the-field.html
[Accessed 03 2018].

Kilburn, J., 2007. Machine maintenance - caring for today's HRSG. *Decentralized Energy.*

Korean Atomic Research Institute, 2009. *Introductory Meeting on the Planned PSI research Project on HTR Graphite Duct Issues.* s.l., Thermal Hydraulics Safety Research Division.

Kowadlo, A. R. &., 2012.
Advanced_airflow_modelling_using_naive_physics_for_odour_localisation, s.l.: Researchgate.

Long, L., 2012. *Ammonium stability and nitrogen isotope fractionations for –NH3 (aq),* Toronto: Couloume Department of Geology, University of Toronto.

Ma, F. Y., 2012. *Corrosive effects of chlorides on metals Department of Engineering Taiwan.* [Online]
Available at: http://cdn.intechopen.com/pdfs/33625.pdf
[Accessed 08 03 2018].

NRC, 2011. *P1000 Design Control Document Rev 19, Tier 2, Chapter 11 Radioactive Waste Management,* s.l.: NRC.

Paans, A., n.d. *Positron Emission Tomography,* Groningen : Groningen University Hospital.

Procon Engineering, 2017. *Boiler acoustic steam leak detection.* [Online]
Available at:
http://www.proconeng.com/pdf/Leak%20Detection%20PDF/Procon%20Boiler%20Leak%20Detection%20Brochure%208%20page%20Iss.%204%20April%2017.pdf
[Accessed 18 March 2018].

Russell, e. a., 2006. *Improving the robustness of Na1ve physics airflow mapping using Bayesian reasoning on a multiple hypothesis tree.,* Victoria, Australia: Monash University.

S.W Liu, W. W. &. C. L., 2017. Failure analysis of the boiler water-wall tube.

Sang-Baik, K., 2009. *Issues and Modeling of Fission Product in HTGR at KAERI.* [Online]
Available at:
https://smr.inl.gov/Document.ashx?path...Int%2FNHDDISSUESKAERI_PSI...pdf
[Accessed 12 January 2018].

Scampini, J., n.d. *Introduction to PET imaging.* [Online]
Available at: https://www.maximintegrated.com/en/app-notes/index.mvp/id/4680
[Accessed 20 January 2018].

Siemens, 2018. *SGT5 8000H Heavy duty gas turbine.* [Online]
Available at: https://www.siemens.com/global/en/home/products/energy/power-generation/gas-turbines/sgt5-8000h.html#!/
[Accessed 03 2018].

Siemens, 2018. *Siemens heavy duty Gas Turbine 8000H.* [Online]
Available at: https://www.siemens.com/global/en/home/products/energy/power-generation/gas-turbines/sgt5-8000h.html#!/
[Accessed 30 June 2018].

Siemens, 2018. *Siemens Products and Services.* [Online]
Available at: https://www.siemens.com/global/en/home/products/energy/power-generation/gas-turbines/sgt5-8000h.html#!/
[Accessed 3/2/2018 February 2018].

Siemens, 2018. *Utility Steam Turbines - proven technology.* [Online]
Available at: https://www.siemens.com/global/en/home/products/energy/power-generation/steam-turbines/utility-steam-turbines.html
[Accessed 03 2018].

Siemens, L. B., 2011. Fast Cycclying and rapid start up. *Modern Power Systems .*

Softflo (Flo++), n.d. *CFD program for modelling industrial fluid flow and heat transfer processes.* [Online]
Available at: http://homepage.usask.ca/~ijm451/finite/fe_resources/node545.html
[Accessed 12 January 2018].

Studdard, B. & Arrington, P., 1992. *Technical Paper BR-1492 Operating experience using acoustic leak detection at Gaston Station,* s.l.: s.n.

Toivonen, e. a., 2013. *Optical detection of KCl vapor and atomic K release from biomass fuels combusted in a single particle reactor.* [Online]
Available at: http://www.ffrc.fi/FlameDays_2013/Presentations/Sorvajarvi.pdf
[Accessed 15 January 2017].

Toivonen, T. S. &. J., 2013. Principles and calibration of collinear photofragmentation and atomic absorption spectroscopy. *Applied Physics B Lasers and Optics.*

Toivonen, T. U. o. T. -. T. S. &. J., 2013. *Optical detection of KCl vapor.* [Online]
Available at: http://www.ffrc.fi/FlameDays_2013/Presentations/Sorvajarvi.pdf
[Accessed 03 2018].

turbine, S. S.-4. h. d. g., 2018. *Technology.* [Online]
Available at: https://www.siemens.com/global/en/home/products/energy/power-generation/gas-turbines/sgt6-5000f.html#!/

UC San Diego school of medicine, 2018. *PET Physics Instrument data analysis.* [Online]
Available at: https://cfmriweb.ucsd.edu/ttliu/be280a_04/BE280A_04_pet.pdf

Universities, O. R. A., 2009. *General Information About K-40.* [Online]
Available at:
https://www.orau.org/ptp/collection/consumer%20products/potassiumgeneralinfo.htm

Watlow Supply, 2018. *Watlowsupply.com.* [Online]
Available at: https://www.watlowsupply.com/Ceramic-Fiber-Heaters-_p_33.html
[Accessed 12 January 2018].

Weigang Lin, C. E. W. P. F. B. H. &. K. D.-J., 1999. *1. Hydrodynamics of a commercial scale CFB boiler-study with radioactive tracer particles. ,* s.l.: Department of Chemical Engineering, Technical University of Denmark..